Structure−Activity Relationships in Peptide Modulators of β-Amyloid Protein Aggregation: Variation in α,α-Disubstitution Results in Altered Aggregate Size and Morphology

Cyrus K. Bett,[†] Johnpeter N. Ngunjiri,[‡] Wilson K. Serem,[†] Krystal R. Fontenot,[†] Robert P. Hammer,[§] Robin L. McCarley,[†] and Jayne C. Garno*,[†]

[†]Department of Chemistry, Louisiana State University, Baton Rouge, Louisiana 70803, [‡]NanoInk, Inc., Illinois Science & Technology Park, 8025 Lamon Ave, Skokie, Illinois 60077, and [§]New England Peptide LLC, 65 Zub Lane, Gardner, Massachusetts 01440

Abstract

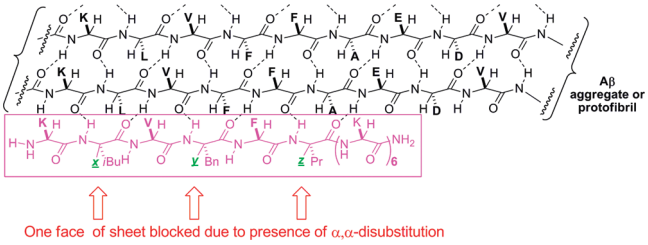

Neuronal cytotoxicity observed in Alzheimer's disease (AD) is linked to the aggregation of β-amyloid peptide (Aβ) into toxic forms. Increasing evidence points to oligomeric materials as the neurotoxic species, not Aβ fibrils; disruption or inhibition of Aβ self-assembly into oligomeric or fibrillar forms remains a viable therapeutic strategy to reduce Aβ neurotoxicity. We describe the synthesis and characterization of amyloid aggregation mitigating peptides (AAMPs) whose structure is based on the Aβ "hydrophobic core" $A\beta_{17-20}$, with α,α-disubstituted amino acids (ααAAs) added into this core as potential disrupting agents of fibril self-assembly. The number, positional distribution, and side-chain functionality of ααAAs incorporated into the AAMP sequence were found to influence the resultant aggregate morphology as indicated by ex situ experiments using atomic force microscopy (AFM) and transmission electron microscopy (TEM). For instance, AAMP-5, incorporating a sterically hindered ααAA with a diisobutyl side chain in the core sequence, disrupted $A\beta_{1-40}$ fibril formation. However, AAMP-6, with a less sterically hindered ααAA with a dipropyl side chain, altered fibril morphology, producing shorter and larger sized fibrils (compared with those of $A\beta_{1-40}$). Remarkably, ααAA-AAMPs caused disassembly of existing Aβ fibrils to produce either spherical aggregates or protofibrillar structures, suggesting the existence of equilibrium between fibrils and prefibrillar structures.

Keywords: β-Amyloid, Alzheimer's disease, amyloid aggregation mitigating peptides, α,α-disubstituted amino acids, fibrils, spherical aggregates

Alzheimer's disease is a progressive neurodegenerative disorder characterized by extracellular plaque deposits and neurofibrillar tangles. The plaque deposits are composed primarily of the natively unfolded amyloid β-peptide (Aβ, containing 39−42 amino acids) that is derived from proteolytic cleavage of the extracellular segment of the transmembrane amyloid precursor protein (APP) (*1*−*3*). The normal physiological concentration of Aβ in the brain is less than 10 nM. However, the critical concentration for Aβ to aggregate in vitro into amylogenic forms is 1−10 μM (*4*, *5*). Several hypotheses as to how Aβ aggregates in the brain at concentrations below the critical nanomolar value include binding/concentration of Aβ to several orders of magnitude by membranes or organelles, lowering of the critical aggregation concentration by decreases in pH or presence of metal ions, and forming covalent adducts between Aβ and oxidative metabolites (*5*−*7*).

Conversion of monomeric Aβ peptide into the aggregated products (oligomers, protofibrils, and fibrils) in the brain is believed to be the vital event in AD pathology (*8*, *9*). Fibrils were initially targeted as the species responsible for neuronal toxicity and cell death (amyloid cascade). More recently, growing evidence suggests that much smaller and soluble oligomeric Aβ species (isolated as dimers, trimers, and tetramers from various sources such as cells, brain homogenates, and in vitro aggregation assays) correlate better with severity of AD than plaques (fibrils) (*3*, *10*−*18*). However, multiple reports have shown protofibrils, fibrils, and oligomers as toxic species (*9*, *12*, *19*−*22*). Therefore, assembly of Aβ into either oligomeric or fibrillic assemblies remains a rational target to reduce Aβ neurotoxicity. In addition, fibril dissolution agents could be possible targets for reducing plaque loads in the brain.

Several approaches aimed at reducing production or clearance of Aβ and its related aggregates in the brain

Received Date: May 6, 2010
Accepted Date: June 25, 2010
Published on Web Date: July 08, 2010

DOI: 10.1021/cn100045q | *ACS Chem. Neurosci.* (2010), *1*, 608–626

Table 1. Mitigators Derived from Modifications of the Aβ Hydrophobic Core (Aβ_{16-20}) and the Ratios Required To Alter the Aβ Assembly Process

peptide design	ratio (inhibitor/Aβ)	resultant aggregate	method	refs
C-terminal lysine hexamer as disrupting element (KLVFFK_6)	2:1	fibrillar with altered morphology, nontoxic	TEM, DLS	(*43*, *44*)
KLVFF dendrimer	4:1	spherical aggregates	TEM, AFM	(*46*)
D-amino acids, KLVFFA	1:1	protofibrils, ill defined aggregates	TEM	(*47*)
KLVFF-aminoethoxyaceticacid	2:1			(*48*)
glycine spacer (RGKLVFFGR)	2:1	no fibrils	TEM	(*49*)
replacement of amide hydrogens with *N*-methyl groups	30:1	spherical aggregates	TEM	(*50*, *51*)
replacement of amide bonds with ester bonds	20:1	nonfibrillar	TEM	(*52*)
replacement of amide bonds with isostructural olefin bonds	substoichiometric or 4:1	no inhibition	ThT	(*53*, *54*)
β-sheet breakers such as proline	20:1	spherical aggregates	TEM	(*55*)

are under development (*23*, *24*). These include inhibition or modulation of proteases involved in the cleavage of Aβ from the amyloid precursor protein (APP) (*25*−*27*), the use of antibody therapy (through passive immunizations with anti-Aβ antibodies (*28*−*30*) and nonantibody-based natural mechanisms) (*31*−*33*), small organic molecules or nonpeptides such as inositols, phenols, and indoles (*26*, *34*−*38*) and peptides (*34*). Interest in peptide-based aggregation mitigators of Aβ aggregation has intensified, because peptides are generally more potent and display higher specificity of action and fewer toxicological challenges than small organic molecules. A number of peptide-based amyloid aggregation mitigating peptides (AAMPs) that alter Aβ aggregation kinetics or aggregate morphologies have been developed. All of these peptide-based mitigators are designed to exploit the self-interacting Aβ central hydrophobic core (Aβ_{16-20}, KLVFF) as a recognition element because the assembly of Aβ oligomers is controlled by initial interaction of hydrophobic side chains in this central hydrophobic core.

Several modifications of the hydrophobic core (Aβ_{16-20}) aimed at designing AAMPs that enhance the disruption of fibril formation or induce fibril disassembly or both have been reported (*39*−*47*). Murphy and Kessling added an oligolysine tail to the Aβ_{16-20} hydrophobic core that enhanced Aβ aggregation rates resulting in kinetically trapped, nontoxic fibrillar species (*41*, *42*). More recently, RG−/−RG amino acid residues added to the N- and C-termini proved to be effective inhibitors of fibril formation and protected SH-SY5Y cells (neuroblastoma cell line) from Aβ toxicity (*48*). Amide backbone modifications of Aβ_{16-20} core with *N*-methyl amino acids (*49*, *50*), ester linkages (*51*), and isostructural *E*-olefin bonds (*52*, *53*) disrupted fibril formation and induced disassembly of preformed fibrils. Also, Soto and co-workers designed the peptide LPFFD containing a single proline residue in the Aβ_{16-20} core, and it disrupted fibril formation, led to disassembly of existing (preformed) fibrils, and increased cell viability (*54*). Although these AAMPs altered the Aβ fibrillization pathway by inducing different Aβ aggregate morphologies, the processes often required unusually high inhibitor/Aβ molar ratios as shown in Table 1.

Our design of AAMPs is based on the Aβ_{16-20} hydrophobic core where some natural amino acids were replaced by the modified analogs (ααAAs). The α-carbon of the natural amino acid was modified by introducing a second similar side chain to form ααAAs. When ααAAs are incorporated in short peptides, they are known to induce stable extended conformations, which are ideal for interacting with Aβ through hydrogen bonding as well as by side-chain interactions. When ααAAs are placed at alternating positions (i, $i+2$, $i+4$), which positions them on the same hydrogen bonding face of the extended peptide, this serves to sterically block the peptide from further hydrogen bonding, hence disrupting fibril propagation. Also, ααAAs with larger side chains impose restrictions on peptides that contain them. Thus, peptides incorporating ααAAs could be better disrupters of β-sheets than proline-containing mitigators (*54*). Peptide mitigators containing ααAAs with methyl side chains have long been known to disrupt β-sheets (*55*). Thus, we hypothesize than mitigators incorporating ααAAs with side chains larger than methyl groups should be more effective disrupters of β-sheets and disassemble preformed fibrils.

We previously communicated that at stoichiometric and substoichiometric concentrations, peptides containing ααAAs alter the Aβ assembly pathway so as to yield nonfibrillic, nontoxic assemblies (*56*). Our two AAMPs (previously denoted as AMY-1 and AMY-2 and having a hydrophilic lysine tail on the C- or N-terminus, respectively) mitigated Aβ_{1-40} fibril formation in a way that ill-defined Aβ_{1-40} aggregates of different size were produced. When AAMP-1 was injected into hippocampus

DOI: 10.1021/cn100045q | *ACS Chem. Neurosci.* (2010), *1*, 608–626

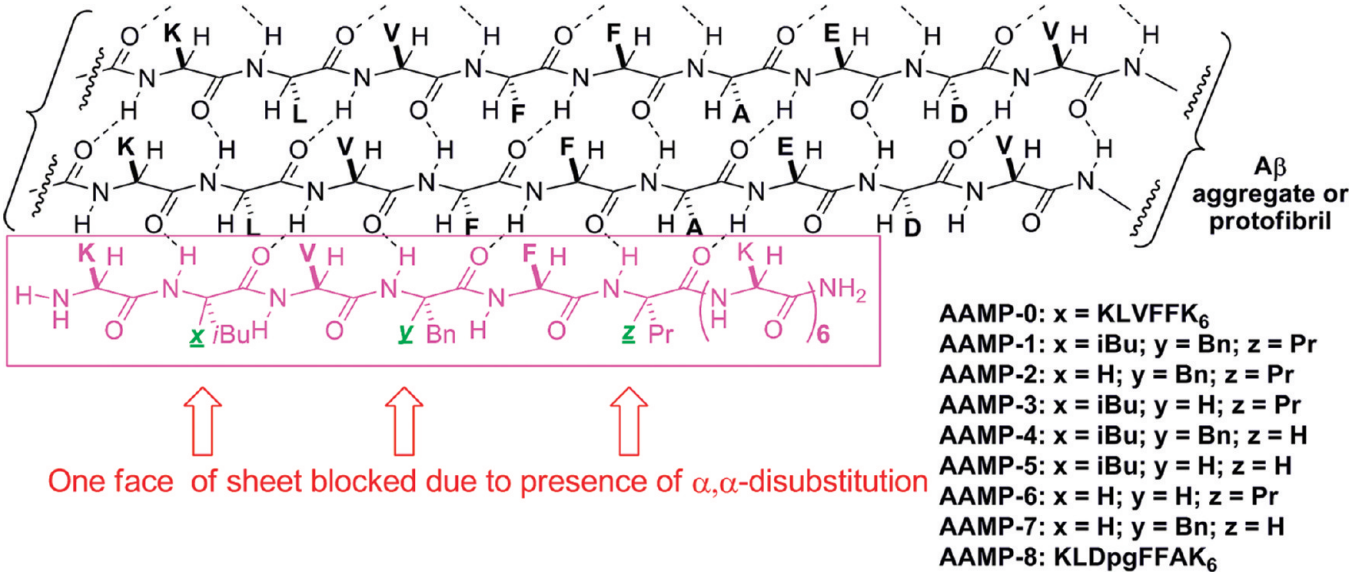

Figure 1. Design of amyloid aggregation mitigating peptides (AAMPs) with α,α-disubstituted amino acids (ααAAs) as disrupters of Aβ assembly. AAMP-0 is the control peptide with no ααAAs. The ααAAs *i*Bu (isobutyl-glycine), Bn (dibenzylglycine), and Pr (dipropylglycine) are analogs of L-natural amino acids leucine, phenylalanine, and alanine, respectively.

of 14-month old APP transgenic mice (TG2576 derived; Swedish mutation) showing age-dependent accumulation of Aβ in the cerebral cortex and hippocampus, it showed a tendency to reduce deposition of Aβ assemblies (*57*). Thus, for optimal use in vivo and improved systemic bioavailability, the molecular weight and charge of AAMP-1 should be greatly reduced. The molecular weight aspect will be addressed in this paper by evaluating the role and position of individual ααAAs. The charge component will be addressed in a separate report because mitigators with a high number of charged residues (lysine) might not penetrate the CNS efficiently. The smaller isoform, $A\beta_{1-40}$, was targeted because it displays slower aggregation kinetics than the longer and more toxic $A\beta_{1-42}$.

Herein, we show that the number and position of ααAAs in the recognition element (Aβ central hydrophobic core) of the original mitigator AAMP-1 (AMY-1) (*56*) is important in determining the effectiveness of the interaction of our AAMPs with Aβ. Also, we further examine the aggregate inhibition role of each ααAA in AAMP-1 by examination of synthetically derived AAMP-1 analogs having ααAAs replaced by their natural amino acid analog (leucine for Dibg, etc). It has been found that the $A\beta_{1-40}$−AAMP interaction dictates the microscopically determined size and morphology differences of the nanoparticles formed. We also show that AAMPs alone do aggregate slowly to yield exclusively spherical, ill-defined particles; this latter observation provides some insight into the mechanism by which the AAMPs disrupt $A\beta_{1-40}$ fibril formation. Furthermore, a major finding is that AAMPs that disrupted fibril formation also led to disassembly of preformed (existing) $A\beta_{1-40}$ fibrils.

Results and Discussion

Design of Amyloid Aggregation Mitigating Peptide

The central hydrophobic region of Aβ (16−20) is responsible for $A\beta_{1-40}$ self-recognition and assembly that leads to the formation of mature fibrils with diameter 7−10 nm (*44*). The self-interacting property of Aβ has been exploited to design disrupters of $A\beta_{1-40}$ fibrillization. For instance, when ααAAs are incorporated into a peptide, they are known to induce extended peptide conformations that are ideal for interaction with Aβ (*58*, *59*). We hypothesize that peptides containing alternating natural amino acids and ααAAs in a β-strand (extended) conformation will have one hydrogen bonding "face" blocked due to the steric hindrance associated with the side chains of ααAAs, and the other face would remain accessible for additional β-strand hydrogen bonds. This design strategy (Figure 1) does not prevent Aβ oligomerization but disrupts additional peptides from adding to one face of the growing β-sheet, thus changing the Aβ fibrillization pathway. Previously, we showed that no fibrils were observed in $A\beta_{1-40}$-AAMP-1 mixtures after 4.5 months of incubation at room temperature (*56*). In the study at hand, we seek to elucidate the relationship between the side-chain functionalities of the ααAAs as well as the positioning and distribution of ααAAs in the recognition element (KLVFFA) of AAMPs and the resulting $A\beta_{1-40}$-AAMP-1 assembly size and morphology. Strategically designed variations of AAMP-1 peptides were synthesized and evaluated (Figure 1). Mitigator AAMP-0 ($KLVFFK_6$) was used as a control peptide, due to its lack of ααAAs but similarly designed backbone to our AAMPs (*41*, *42*).

DOI: 10.1021/cn100045q | *ACS Chem. Neurosci.* (2010), *1*, 608–626

When bound to amyloid fibrils, thioflavin T dye (ThT) undergoes a red shift of its absorbance maximum from 342 to 442 nm and a characteristic enhanced fluorescence signal at 482 nm (*60*, *61*). Binding of ThT dye to Aβ fibrils is complete within 1 min and does not interfere with Aβ aggregation (*61*). Thus, ThT fluorescence is commonly used to monitor for the presence of Aβ fibrils and their rates of formation. It has also been shown that ThT can bind to certain amorphous aggregates to produce an increased fluorescence signal (*62*, *63*). Therefore, increases in ThT fluorescence are insufficient to monitor Aβ fibril formation/disruption. The combination of complementary methods such as circular dichroism (CD), AFM, and TEM is needed to probe mitigation of Aβ_{1-40} fibril formation by designed inhibitors because such combination can reveal the conformation, size, length, and morphology of resulting aggregates. We emphasize investigations using high-resolution AFM in the present work because of the unique capability of readily probing early aggregation products (small oligomers) and providing three-dimensional characteristics of Aβ assembly products (*64*−*69*).

Aggregation of Aβ_{1-40} has been proposed to proceed via a nucleation-dependent polymerization mechanism wherein a nucleus is first formed and then grows in size by addition of monomeric Aβ_{1-40} (*6*, *70*). Formation of nuclei from truly monomeric solutions of Aβ_{1-40} is a rate-limiting step, and the presence of Aβ_{1-40} seed nuclei greatly accelerates aggregation as a result of the presence of the kinetically more expedient pathway. Thus it is critical to pretreat Aβ_{1-40} materials to ensure that the initial solutions used for mitigator studies possess monomeric Aβ_{1-40} (*71*).

Effect of AAMPs on Aβ_{1-40} ThT Fluorescence

As shown in Figure 2, Aβ_{1-40} solutions aged in the presence of equimolar AAMPs display time-dependent increases in ThT fluorescence, an observation that is consistent with the formation of aggregates. A small but measurable increase (3−18%) in ThT fluorescence is noted in the case of mitigators aged alone, indicating the formation of a small amount of ThT-active species, perhaps AAMP aggregates or assemblies.

A significant observation was the decrease in total ThT fluorescent signal after 3 months of incubation at room temperature in most of the AAMP−Aβ_{1-40} mixtures. We speculate that the decreased fluorescence that is observed results from continuous aggregation of these mixtures that leads to the formation of larger assemblies that eventually precipitate out of solution. In addition, results from the control peptide (AAMP-0) that is known to enhance Aβ_{1-40} self-assembly and yield a network of fibrils (*42*) were compared with those of our AAMPs to probe the importance of ααAA presence in inhibitor make up. The fluorescence of a mixture of

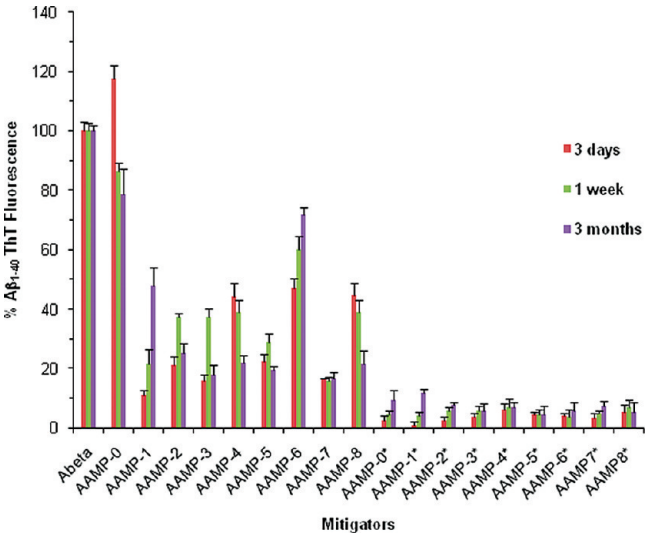

Figure 2. Assembly of Aβ_{1-40} in the presence of ααAA-AAMPs. Time-dependent ThT fluorescence monitoring of Aβ_{1-40} assembly in the presence or absence of the various AAMPs. Fluorescence (ThT) was set arbitrarily to 100% relative to Aβ_{1-40}. The * denotes mitigators aged alone.

Aβ_{1-40} and AAMP-0 is 120% that of Aβ_{1-40} alone after 3 days of incubation, and 80% of Aβ_{1-40} alone for 3 months aging times. These observations are consistent with previous reports describing enhanced Aβ_{1-40} fibrillogenesis with this material (*41*, *42*).

A significant reduction in Aβ_{1-40} ThT fluorescence is observed when Aβ_{1-40} is aged with an equimolar mixture of ααAA-AAMPs. Mitigators AAMP-1, AAMP-2, AAMP-3, AAMP-4, AAMP-5, AAMP-7, and AAMP-8 exhibit a reduction of ThT fluorescence between 50% and 80% relative to that of Aβ_{1-40} alone, even after 3 months of aging. Peptide mitigator AAMP-6 displayed a reduced ThT fluorescence of 40% and 20% relative to Aβ_{1-40} after 3 days and 3 months aging, respectively. Comparison of the sequence of AAMP-6 with other AAMPs that showed reduction in ThT fluorescence between 50% and 80% relative to the control reveals the importance of steric effects and position of ααAAs relative to the recognition element.

Concentration-dependent changes for the disruption of the Aβ_{1-40} fibrillization process were examined by fixing the concentration of Aβ_{1-40} to 40 μM and adding selected AAMPs at 4, 40, and 400 μM levels. Samples were removed at 3 and 7 days of incubation and analyzed with ThT fluorescence assay. Aggregation of Aβ_{1-40} into ThT-positive assemblies was disrupted in a concentration-dependent manner (see Supporting Information, Figure S1). The data also reveals that even at substoichiometric concentration of AAMP-3 (4 μM), reduction in ThT fluorescence was observed indicating the disruption of amyloid fibril formation, resulting possibly in nonfibrillic assemblies. Also, selected AAMPs

DOI: 10.1021/cn100045q | *ACS Chem. Neurosci.* (2010), *1*, 608–626

Table 2. Wavelength and Corresponding Minimum and Maximum Ellipticities of CD Spectra of AAMPs Alone, $A\beta_{1-40}$ Alone, and 1:1 $A\beta_{1-40}$-AAMP Mixtures (40 μM)[a]

		with Aβ (1:1)							
		3 days aging				7 days aging			
entry	AAMP	λ (nm)	min/max [θ]	λ (nm)	min/max [θ]	λ (nm)	min/max [θ]	λ (nm)	min/max [θ]
1	$A\beta_{1-40}$	206	−4.89	220	−0.275	198	5.03	214	−14.53
2	AAMP-0	204	−31.34	219	−1.821	195 (199)	−14.66 (−39.86)	207 (221)	2.4 (3.98)
3	AAMP-2	202	−20.88	218	21.10	200 (199)	−9.89 (−36.271)	218 (217)	0.46 (15.83)
4	AAMP-3	202	−50.18	220	−4.12	206 (195)	0.297 (−29.63)	220 (213)	−3.25 (15.22)
5	AAMP-4	204	−18.43	221	2.82	203 (202)	−7.93 (−22.47)	213 (215)	−2.95 (11.83)
6	AAMP-6	202	−50.18	218	−4.41	202 (202)	−8.27 (−40.96)	219 (219)	2.35 (14.12)
7	AAMP-7	202	−25.34	222	−5.85	200 (202)	−11.20 (−22.47)	224 (221)	−0.69 (13.95)

[a] Values in parentheses are for AAMPs aged alone after 1 week. Molar ellipticity [θ] units = deg cm^2 $dmol^{-1}$.

were tested against $A\beta_{1-42}$, which is more prone to aggregation and toxic effects. The mitigators tested were found to disrupt $A\beta_{1-42}$ assembly similarly as for $A\beta_{1-40}$ (see Supporting Information, Figure S2).

Effect of ααAA-AAMPs on the Secondary Structure of $A\beta_{1-40}$ as Probed by Circular Dichroism

To examine the effect of ααAA-AAMPs on $A\beta_{1-40}$ assemblies, far-UV CD spectroscopy was employed. The CD spectra of monomeric AAMPs and $A\beta_{1-40}$ have a characteristic, intense minimum and a maximum near 200 and 220 nm, respectively, observations that are consistent with a random coil conformation. After a week of aging AAMPs alone at 37 °C, the spectrum found for the random coil conformation of AAMPs remained unchanged, albeit with weaker intensities (Table 2).

Our CD observations for $A\beta_{1-40}$ (Table 2, entry 1) reveal that the time course of forming the β-sheet conformation is consistent with previously reported β-sheet-rich assemblies (*56*, *72*). The structure of $A\beta_{1-40}$ incubated alone changed from random coil (monomeric) to β-sheet after 7 days of incubation (minimum at 214 nm). In contrast, equimolar mixtures of AAMPs and $A\beta_{1-40}$ lead to an unusual CD signature (see Supporting Information, Figure S3) having characteristics of both random coil and β-sheets (Table 2, entries 2−7), these results are consistent with those from our previous CD study of $A\beta_{1-40}$AAMP-1 mixtures (*56*).

Atomic Force Microscopy Evaluation of Aggregate Morphologies of AAMPs Aged Alone

All AAMPs aged alone gave rise to the occasionally observed spherical, bead-like aggregate with mean height range of 4−10 nm (see Supporting Information, Figure S4). The AFM-observed absence of fibrils or highly organized assemblies is consistent with CD results that exhibit little change in the random coil conformation with maxima around 220 nm and minima at 200 nm after 1 week of incubation. Also, the minimal ThT fluorescence observed with AAMPs aged alone relative to $A\beta_{1-40}$ suggests that the nanostructures formed are not β-sheet-rich. We speculate that hydrophobic forces are stronger than hydrogen bonding forces in the AAMPs in buffered aqueous milieu, and as a result, spherical AAMP aggregate morphologies were produced. The small-sized spherical aggregates formed when AAMP-1 was aged alone for 3 days may explain the cell toxicity we have reported previously (*73*). It is posited that the observed spherical beads of the AAMPs might act as seeds for $A\beta_{1-40}$ aggregation, thereby allowing for the ready formation of $A\beta_{1-40}$ fibrils. However, this assumes that the AAMP bead-like aggregates coexist in the presence of monomeric $A\beta_{1-40}$. In addition, fibrils of $A\beta_{1-40}$ were not observed (*vide infra*) in the presence of the AAMPs, suggesting that the possible existence of AAMP bead-like aggregates does not lead to seeded growth of $A\beta_{1-40}$ fibrils.

Atomic Force Microscopy Evaluation of Aggregate Morphologies of $A\beta_{1-40}$ Aged Alone and with the Various AAMPs

We used AFM to characterize $A\beta_{1-40}$ or $A\beta_{1-40}$-AAMP-1 sample aliquots taken at the same time intervals as those used for ThT fluorescence assays. We also used TEM to confirm AFM observations (see Supporting Information, Figure S5). Images obtained from AFM topographs of aliquots taken at different aging times for $A\beta_{1-40}$ and in presence of AAMP-0 and AAMP-1 are shown in Figure 3. As expected, fibrils were the predominant structures observed after 1 week of aging $A\beta_{1-40}$ alone (Figure 3A). These fibrils had a mean height of 4 ± 2 nm, which is smaller than the reported mean height of about 7−10 nm for mature $A\beta_{1-40}$ fibrils (*69*, *74*). The presence of smaller sized fibrils is an indication that protofibrils and some immature fibrils predominate at the early stage, which is supported by height distribution analysis that leads to

DOI: 10.1021/cn100045q | ACS Chem. Neurosci. (2010), 1, 608–626

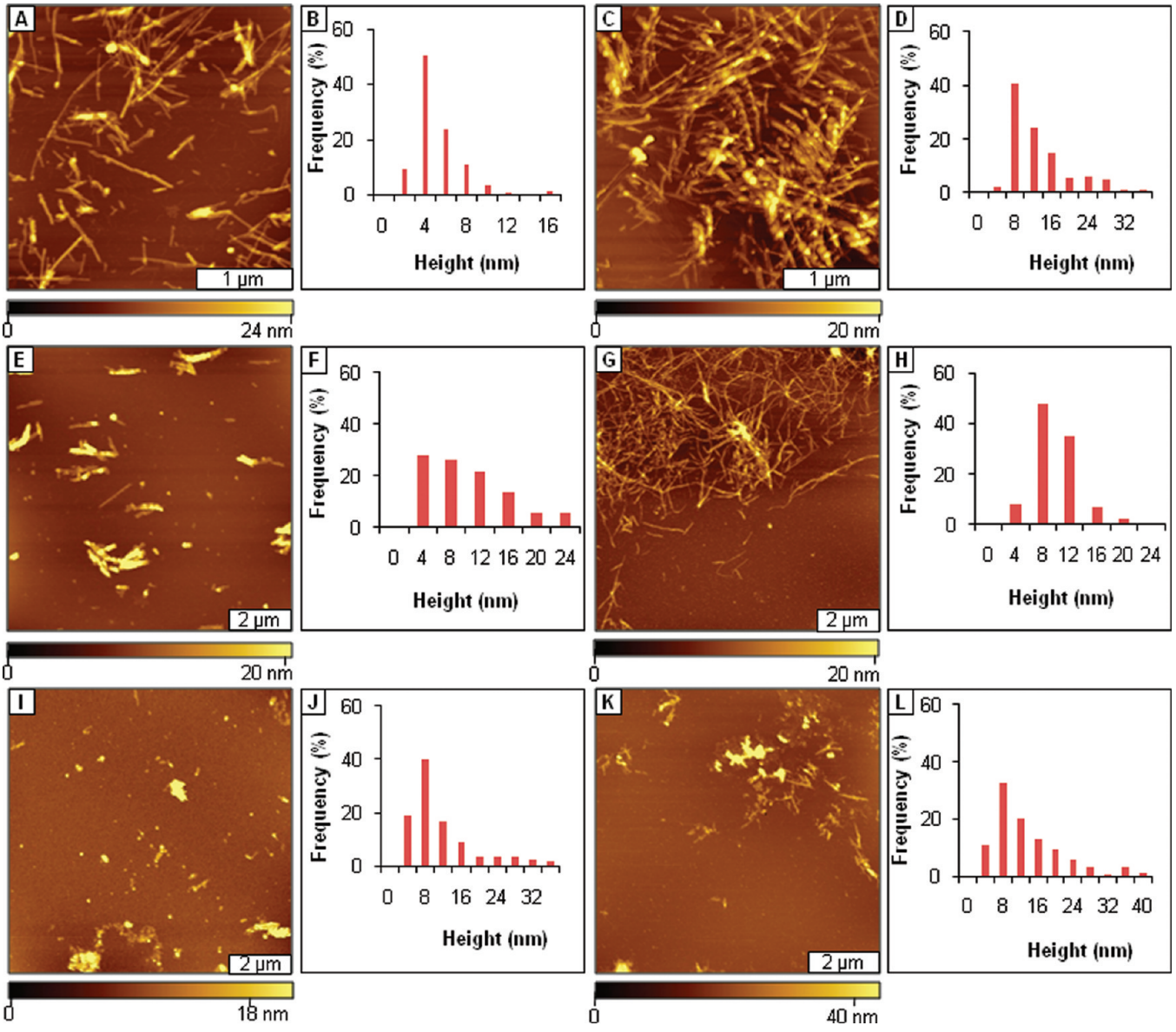

Figure 3. Aggregation of Aβ_{1-40} with and without AAMPs: (A) fibrils formed by Aβ_{1-40} alone after 1 week of incubation; (B) height distribution histogram for panel A; (C) fibril bundles formed by Aβ_{1-40} alone after 3 months of incubation; (D) height distribution histogram for panel C; (E) protofibrils formed after 3 days of Aβ_{1-40} aggregation mitigated by AAMP-0; (F) height distribution histogram for panel E; (G) fibril network formed after 1 week of Aβ_{1-40} aggregation mitigation by AAMP-0; (H) height distribution histogram for panel G; (I) mixture of spherical and linear aggregates formed after 1 week of Aβ_{1-40} aggregation with mitigation by AAMP-1; (J) height distribution histogram for panel I; (K) spherical assemblies and protofibrils observed after 3 months of Aβ_{1-40} aggregation with mitigation by AAMP-1; (L) height distribution histogram for panel K.

observation of fibrils with 2−4 nm diameters composing ≥60% of total fibrils (Figure 3B). In contrast, bundles of fibrils (Figure 3C) were the predominant species observed after 3 months of incubation. An interesting AFM artifact from a double tip is apparent in Figure 3C; however the shapes of the fibrils can be well resolved for this topography frame. The mean height of the fibrils in the bundles was 11 ± 7 nm, and more than 70% of these bundled fibrils had heights ranging from 4 to 12 nm (Figure 3D) indicating mature fibrils (7−10 nm) had formed.

The assembly of Aβ_{1-40} into fibrils is consistent with the proposed hierarchical assembly model (HAM model), which predicts that protofilaments predominate at earlier incubation stages while protofibrils and fibrils are detected later. The HAM model also predicts that protofibrils and fibrils will exhibit periodicity, variations in height, branching, and clumping at various stages of fibrillization. The unique distribution of fibril morphologies that is observed after 3 months of incubation is consistent with fibril clumping as predicted by the HAM model (*75*, *76*).

DOI: 10.1021/cn100045q | *ACS Chem. Neurosci.* (2010), *1*, 608–626

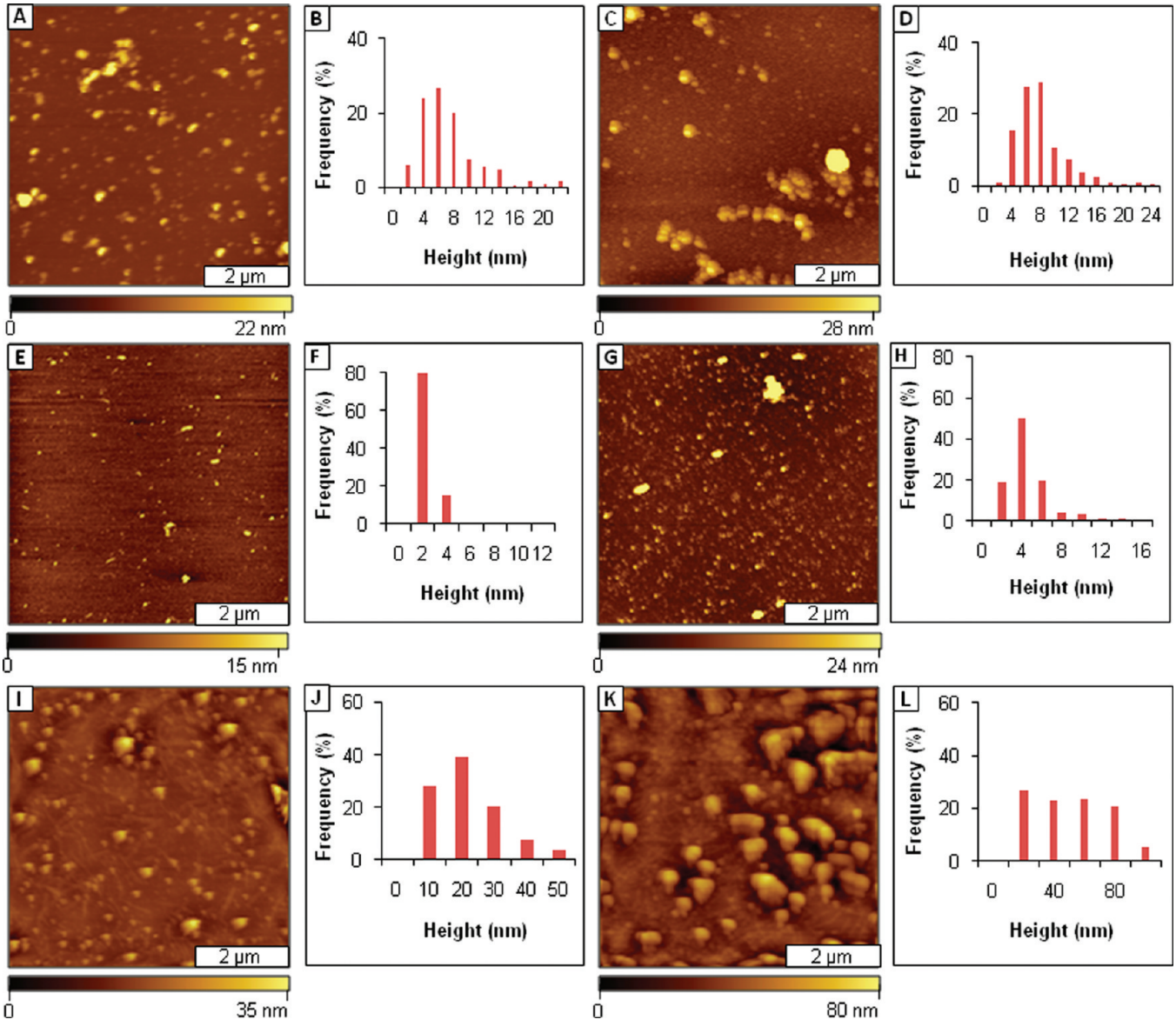

Figure 4. Disruption of Aβ_{1-40} fibril formation by AAMPs with two ααAAs: (A) globular aggregates formed after 7 days aging Aβ_{1-40} in presence of AAMP-2; (B) corresponding height distribution analysis; (C) aggregates formed after 3 months aging Aβ_{1-40} in presence of AAMP-2; (D) corresponding height distribution; (E) spherical aggregates formed after 1 week aging Aβ_{1-40}-AAMP-3 mixture; (F) height analysis for panel E; (G) spherical aggregates after 3 months aging Aβ_{1-40}-AAMP-3 mixture; (H) corresponding height analysis; (I) mixture of spherical aggregates and protofibrils formed after 7 days aging Aβ_{1-40} in the presence of AAMP-4; (J) corresponding height distribution analysis for panel I; (K) after 3 months aging Aβ_{1-40} in the presence of AAMP-4; (L) matching height distribution histogram.

Importance of Using ααAAs as Disrupting Elements: Effect of Three ααAAs on Aβ_{1-40} Fibril Formation

The significance of ααAAs in disrupting fibril formation was evaluated by aging equimolar mixtures of Aβ_{1-40} with AAMP-0 (no ααAAs) and AAMP-1 (with ααAAs). For instance, after 3 days of aging Aβ_{1-40}-AAMP-0 mixtures, protofibrils (Figure 3E) with mean height of 9 ± 6 nm were the main structures observed. A dense network of fibrils (Figure 3G) with mean height of 9 ± 3 nm was observed after 1 week of aging. The height histograms possess time-dependent increases in fibril heights (Figure 3F,H). In contrast, mixtures of protofibrils and spherical aggregates (Figure 3I) with a mean height of 10 ± 8 nm were observed with AAMP-1 after 1 week of incubation, and rod-like structures (Figure 3K) were formed after 3 months with a slight increase in mean height as displayed in Figure 3J,L.

The AAMP-0 peptide (no ααAAs) was used as a control sample for evaluating the effects of ααAAs in the mitigator backbone. This peptide (AAMP-0) was shown previously to enhance the rate of aggregation of Aβ_{1-40} and give rise to dense networks of fibrils (*42*). The enhanced Aβ_{1-40} aggregation rates may also lead to

DOI: 10.1021/cn100045q | *ACS Chem. Neurosci.* (2010), *1*, 608–626

thicker (taller) fibrils compared with Aβ_{1-40} fibrils from its solitary incubation. The structural design for AAMP-0 and our AAMPs are similar except for ααAAs incorporated in the latter (for example, Dbg for Phe, etc). The peptide mitigator AAMP-1 was previously shown to block Aβ_{1-40} fibrillization even after 4.5 months of incubation at room temperature (*56*). The different aggregate morphology observed for Aβ_{1-40} aggregation mitigated by AAMP-0 (fibrils) compared with ααAA-containing AAMP-1 (mixture of spherical aggregates and rod-like structures) reinforces the contrast in using ααAA-containing AAMPs to disrupt fibril formation. The results for AAMP-1 with further characterization of the sizes and morphologies of nanostructures formed at different stages of aggregation using high-resolution AFM are presented in Figure 3I,K. The AAMP-1 analogs were screened for their ability to disrupt Aβ_{1-40} assembly compared with the original mitigator (AAMP-1).

Effects of AAMPs Containing Two ααAAs on Aβ_{1-40} Fibril Formation

When AAMP-1 analogs with two ααAAs were aged with equimolar Aβ_{1-40}, assemblies with different heights and morphologies were formed, and the size/morphology type observed being related to the side-chain functionality of the ααAAs used. Spherical aggregates (Figure 4A) with mean heights of 8 ± 4 nm (60% of the particles with height range of 4−8 nm, Figure 4B) were observed after 1 week of aging Aβ_{1-40}-AAMP-2 mixtures. The spherical morphology of the aggregates did not change after 3 months incubation, but aggregates were observed to coalesce, forming in some cases aggregate strings (Figure 4C). The only significant change was the slight increase in mean heights (9 ± 4 nm) as shown by height distribution analysis (Figure 4D). Compared with AAMP-2, smaller sized spherical aggregates (Figure 4E) with mean height 2 ± 1 nm were formed from co-incubation of Aβ_{1-40} with equimolar AAMP-3. The same morphology was observed after 3 months incubation (Figure 4G) but with a larger mean height (4 ± 2 nm) as shown by AFM cursor analysis (Figure 4F,H). Mixtures of ill-defined aggregates and protofibrils/fibrils visible in the background) with mean height of 18 ± 9 nm (Figure 4I) formed after 1 week of Aβ_{1-40} mitigation by AAMP-4 compared with mostly spherical particles observed after 3 days of incubation. After 3 months of incubation, the mean height of the particles (Figure 4K) more than doubled (43 ± 25 nm) with maximum height spanning to 1 μm as shown in Figure 4J,L. The particles for AAMP-4 appear to have a triangular shape attributed to tip-sample convolution. The convolution results from imaging very tiny, sharp asperities on the sample surface using a much larger tip, thereby yielding a regular printed artifact in the image. The height information will be reliable; however the lateral features result from a convolution of the tip shape.

The disruption of fibril formation by AAMPs with two ααAAs is an important finding in that these AAMPs portrayed the same or better disruptive properties as the original AAMP-1 peptide with three ααAAs. The more interesting aspect of their disruption is the relation between size and morphology of the particles formed and the side chain functionality of incorporated ααAAs. Larger particles with similar morphology were formed from Aβ_{1-40} aggregation mitigated by AAMP-2 and AAMP-4, compared with AAMP-3. The difference in observed heights could be attributed to the side chain functionality of the ααAAs incorporated in AAMP-2 (Dbg and Dpg), AAMP-3 (Dibg and Dpg), and AAMP-4 (Dbg and Dibg). Notably, Dbg (aromatic)-containing AAMPs (AAMP-2 and AAMP-4) formed larger particles compared with AAMP-3 without Dbg. Thus incorporation of the additional aromatic side chain in Dbg-containing AAMPs may play a role in determining the size and morphology of the resultant nanoparticles, because aromatic residues are believed to supply energy, order, and directionality (*77*, *78*) to the Aβ assembly process during fibril formation through aromatic side-chain stacking interactions.

Hydrophobic or steric effects from ααAAs may also contribute to the size and morphology of structures formed. For instance, larger spherical aggregates with a few protofibrils/fibrils were formed with AAMP-4 compared with mainly spherical aggregates for AAMP-2. The different sizes and morphologies of particles formed can thus be related to the combination of the ααAAs used in each AAMP. They both have aromatic Dbg and a different second ααAAs (Dpg and Dibg for AAMP-2 and AAMP-4, respectively). Thus, steric or hydrophobicity differences between Dpg (*n*-side chains) and Dibg (branched side chains) has influenced the size and morphology of the assemblies formed.

Positioning of ααAAs relative to each other in the AAMP sequence could influence the size and morphology of assemblies formed. One of the ways to induce extended peptide conformations required for the interaction with Aβ in short model peptides is to use ααAAs with larger side-chain groups. For instance, smaller particles were formed by Aβ_{1-40} mitigation by AAMP-3 compared with either AAMP-2 or AAMP-4. The two ααAAs are in an *i*, *i* + 2 orientation in AAMP-2 and AAMP-4 compared with an *i*, *i* + 4 arrangement in AAMP-3. Other examples of *i*, *i* + 2 design mitigators that were designed by replacement of amide backbone include *N*-methyl groups, ester linkages, and isostructural *E*-olefins, all of which were shown to mitigate fibril formation (*49*, *51*, *52*). Thus placement of the disrupting elements on the same hydrogen bonding face is more crucial for the mitigators to disrupt fibril formation than

DOI: 10.1021/cn100045q | *ACS Chem. Neurosci.* (2010), *1*, 608–626

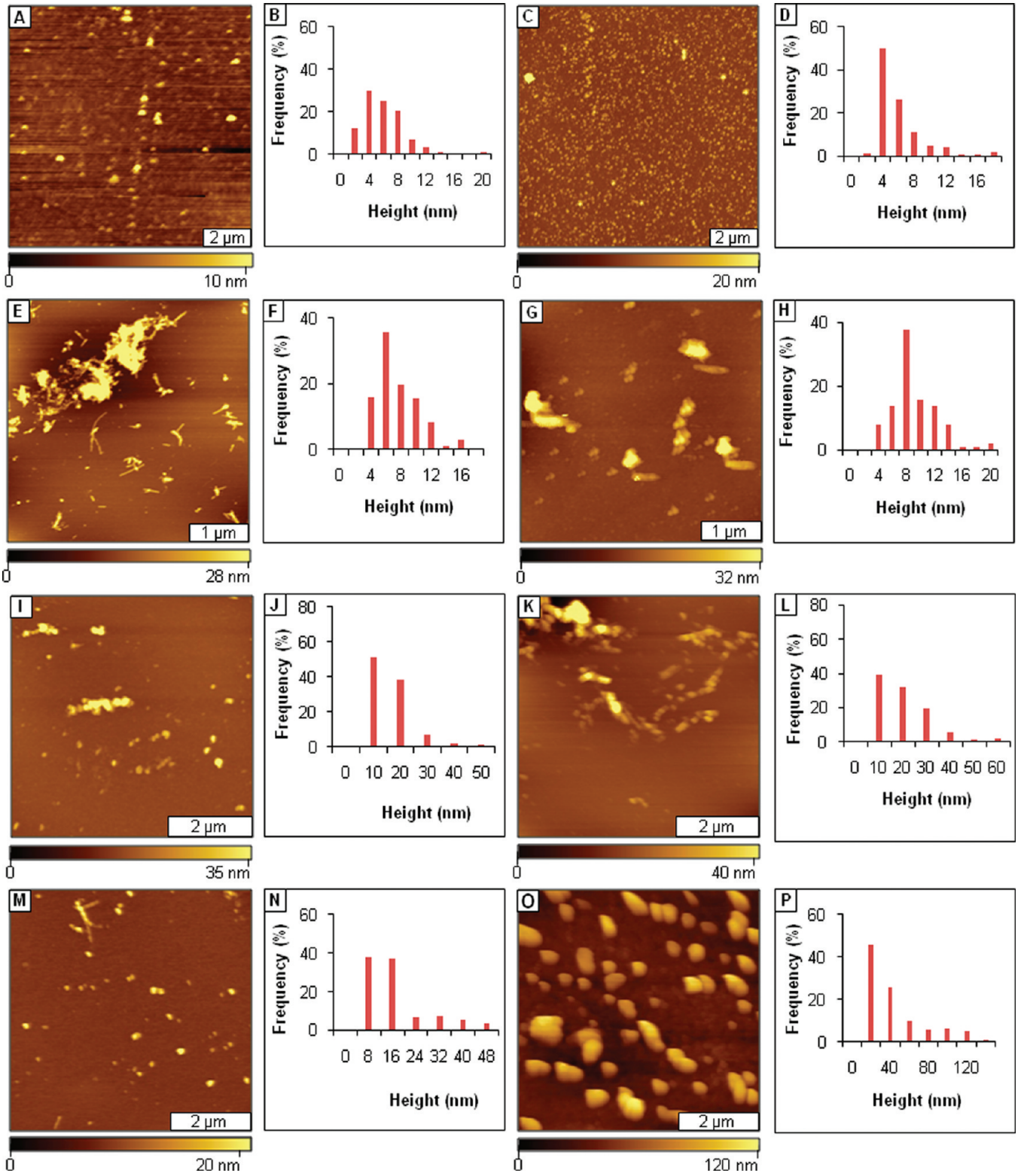

Figure 5. Topographic AFM images showing disruption of $A\beta_{1-40}$ fibril formation by AAMPs with one ααAA: (A) view of nonfibrillic assemblies formed after 1 week $A\beta$ aggregation mitigation by AAMP-5; (B) corresponding height distribution; (C) view after 3 months mitigation by AAMP-5; (D) height analysis for panel C; (E) progressive AFM view of rod-like fibrils detected after 1 week of aging $A\beta_{1-40}$-AAMP-6 mixture; (F) corresponding height distribution; (G) view after 90 days of aging $A\beta_{1-40}$-AAMP-6 mixture; (H) height distribution analysis for panel G; (I) view of spherical and protofibrils/fibrils (background) formed by $A\beta_{1-40}$-AAMP-7 mixture after 1 week aging; (J) corresponding height analysis; (K) view after 90 days aging of $A\beta_{1-40}$-AAMP-7 mixture; (L) height analysis for panel K; (M) view of spherical particles formed by $A\beta_{1-40}$ aggregation mitigation by AAMP-8; (N) corresponding height distribution; (O) view after 3 months aggregation mitigation by AAMP-8; (P) height analysis for panel O.

DOI: 10.1021/cn100045q | ACS Chem. Neurosci. (2010), 1, 608–626

their arrangement. In addition, based on our findings with ααAAs, the number of other disrupting elements reported such as *N*-methylated derivatives and ester linkages could be reduced without affecting their disruptive properties.

Effects of AAMPs with One ααAA on Aβ_{1-40} Fibril Formation

The role of AAMPs with only one ααAA in the mitigation of Aβ_{1-40} aggregation was examined by aging Aβ_{1-40} in the presence of equimolar amounts of AAMP-5 (Dibg), AAMP-6 (Dbg), and AAMP-7 (Dpg). Globular particles were observed to form with AAMP-5 (Figure 5A), which were stable (no fibrils) after 3 months of aging (Figure 5C). Height analysis shows that the percentage of the particles with heights ranging from 4 to 6 nm increased from ~30% for 1 week of incubation to over 50% after 3 months of aging (Figure 5B,D). Co-incubation of Aβ_{1-40}-AAMP-6 mixture produced protofibrillar structures and rod-like fibrils (Figure 5E) after 1 week. The protofibrils (Figure 5G) observed after 3 months of incubation had increased in mean height as displayed by height analysis showing a 2-fold increase in the percentage of particles with heights of 4−6 nm compared with after 1 week (Figure 5F,H). Aging of Aβ_{1-40} with equimolar amounts of AAMP-7 resulted in mainly spherical particles after 3 days. However, a mixture of spherical aggregates and fibrils/protofibrils (Figure 5I) in the background were detected after 1 week of incubation with over 50% of the particles with heights ranging from 1 to 10 nm (Figure 5J). After 3 months of aging, the morphology of the particles (Figure 5K) did not change, but their sizes increased as shown by the increase in the percentage of particles with larger heights (Figure 5L). Spherical aggregates (Figure 5M) with mean heights of 10 ± 5 nm were formed from Aβ_{1-40} mitigation by AAMP-8 after aging for 1 week. Surprisingly, after 3 months, spherical aggregates (Figure 5O) observed earlier have increased in size to greater than a micrometer in some cases, as shown by AFM height analysis (Figure 5N,P).

Results from Aβ_{1-40} mitigation by AAMPs with one ααAA further confirms that side chain functionality of incorporated ααAAs influences the size and morphology of the resulting nanoparticles. For example, the different morphology of the particles observed in AAMP-5 compared with AAMP-6 is because of the steric difference between the ααAAs incorporated: spherical aggregates formed with AAMP-5, which incorporates the more sterically hindered Dibg (isobutyl side chains), compared with rod-like fibrils in AAMP-6, which contains the less sterically hindered Dpg (*n*-propyl side chains). In addition, the size and morphology of fibrils formed by AAMP-6 were different from those of Aβ_{1-40} alone. Fibrils formed by AAMP-6 had larger mean heights (7 ± 3 nm) and smaller lengths (≤1 μm in length)

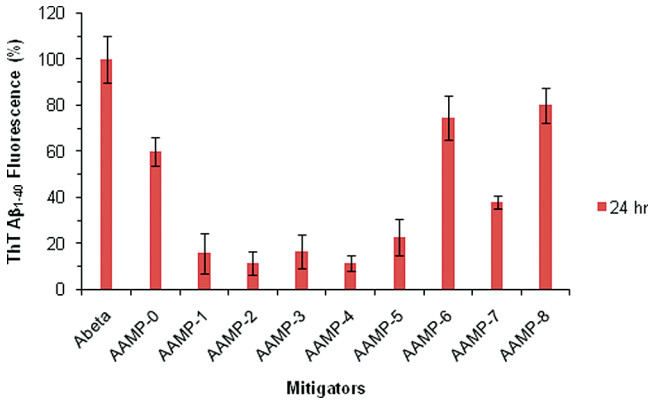

Figure 6. Disassembly of Aβ_{1-40} preformed fibrils. ThT fluorescence of Aβ_{1-40} fibril disassembly by the various AAMPs after 24 h incubation at 37 °C while shaking.

compared with mature Aβ_{1-40} fibrils, which were smaller in mean height (4 ± 2 nm) and several micrometers in length. The short fibril lengths suggest lateral interactions of protofilaments rather than the intertwining commonly identified during amyloid fibril formation, which can also be because of a slower growth rate of protofilaments by elongation and dissociation of monomers. The branching and polymorphic nature of the fibril lengths observed may have been caused by the interactions between protofibrils of unequal lengths (*76*).

Positioning of the ααAAs relative to KLVFF core sequence also influences the morphology of the resulting nanoparticles. The core sequence KLVFF has been shown to be critical for the inhibitor peptide to interact with Aβ. Thus, mitigators with ααAAs placed outside this core sequence should have less influence on the interaction with Aβ compared with mitigators with ααAAs incorporated into this region. An example is the different morphology of particles formed from Aβ_{1-40} mitigation by AAMP-8 (nonfibrillic assemblies) with Dpg incorporated in the KLVFF core (KLDpgFFAK$_6$) compared with AAMP-6 (rod-like fibrils) with Dpg outside the KLVFF core (KLVFFDpgK$_6$). We speculate that the AAMPs with ααAAs incorporated into the binding motif resulted in increased side-chain to side-chain hydrophobic interactions with the homologous core of Aβ. Thus, blocking one face from interchain hydrogen bonding disrupts the Aβ aggregation pathway.

Interestingly, Aβ_{1-40} aggregation mitigated by AAMP-7 with aromatic Dbg yielded spherical aggregates after 3 days of aging. However, after 1 week of incubation a mixture of spherical particles and protofibrils/fibrils in the background with very different morphology relative to Aβ fibrils were formed. This was an unexpected result since it was predicted to disrupt formation of fibrillar structures similar to AAMP-5, which incorporates Dibg. A plausible explanation for the different morphology of

DOI: 10.1021/cn100045q | *ACS Chem. Neurosci.* (2010), *1*, 608–626

Table 3. Effect of Various AAMPs on $A\beta_{1-40}$ Disassembly

			aggregate type after 24 h			
entry	mitigators	α,α-disubstituted amino acid	dominant structures	mean height (nm)	isolated structures	mean height (nm)
1	$A\beta_{1-40}$		fibrils	6 ± 3		
2	AAMP-0		fibrils	5 ± 3	spherical	6 ± 2
3	AAMP-1	Dibg, Dbg, Dpg	spherical	6 ± 3	fibrils	11 ± 6
4	AAMP-2	Dbg, Dpg	spherical	3 ± 1	fibrils	12 ± 5
5	AAMP-3	Dibg, Dpg	spherical	8 ± 5	fibrils	8 ± 3
6	AAMP-4	Dbg, Dibg	spherical	11 ± 8	fibrils	5 ± 3
7	AAMP-5	Dibg	spherical	5 ± 4	fibrils	5 ± 2
8	AAMP-6	Dpg	fibrils	7 ± 2	spherical	5 ± 3
9	AAMP-7	Dbg	spherical	11 ± 6	fibrillar	5 ± 3
10	AAMP-8	Dpg	spherical	11 ± 8	fibrillar	9 ± 5

particles formed by the two mitigators is the aromatic nature of Dbg versus Dibg. This could be due to the enhanced aromatic-stacking interactions asserted by the extra aromatic residue. After 3 days of incubation, AAMP-4 and AAMP-7 disrupted fibril formation. However, after 1 week of incubation, a mixture of spherical particles and protofibrils/fibrils were observed. This indicates that higher ratios of AAMP to $A\beta_{1-40}$ are needed to prevent fibril formation.

$A\beta_{1-40}$ Fibril Disassembly

Several laboratories have reported that a dynamic equilibrium exists between $A\beta_{1-40}$ monomers/dimers and fibrils (*54*, *79*). Thus, a viable strategy to mimic possible dissolution of plaque deposits commonly present in the brains of patients with AD is to screen for compounds that can bind to preformed fibrils, shifting the equilibrium toward prefibrillar species. Soto (*54*, *80*) and Meredith (*49*, *50*) have shown that peptides that incorporate proline (β-sheet breaker) and *N*-methylated amino acids have the ability to disassemble mature $A\beta_{1-40}$ fibrils (*49*, *50*, *54*). The design of *N*-methylated peptides and our ααAA-containing AAMPs are similar in that both were designed to block one hydrogen-binding face thus preventing β-sheet stacking and extension. Therefore, we hypothesized that ααAA-containing AAMPs should also disassemble preformed fibrils because of the more bulky side chains, compared with the methyl group in *N*-methylated peptides.

$A\beta_{1-40}$ Fibril Disassembly as Judged by Thioflavin T Fluorescence

To assess the ability of AAMPs to disassemble preformed fibrils, $A\beta_{1-40}$ was aged for 6 days at 37 °C while shaking. The mature fibrils that formed were mixed with the various AAMPs at 1:1 molar ratio (40 μM final concentration) and incubated while shaking for 24 h. The extent of disassembly was measured by ThT fluorescence. Results of ThT fluorescence for the disassembly of preformed fibrils by the various AAMPs after 24 h incubation are presented in Figure 6 as %ThT fluorescence relative to that of $A\beta_{1-40}$ fibrils.

The general reduction in ThT fluorescence $A\beta_{1-40}$-AAMP mixtures mixtures relative to that of $A\beta_{1-40}$ alone indicates that fibril disassembly occurred. For instance, AAMP-1, AAMP-2, AAMP-3, and AAMP-4 reduced Aβ ThT fluorescence by nearly 80%. This is comparable to the disassembly of $A\beta_{1-40}$ fibrils reported for β-sheet breaker peptide (LPFFD) (*54*), RGTFEGKF peptide (*81*), and *N*-methylated peptides (*49*−*51*), although this was at lower AAMP ratios. Coincidentally, these same mitigators disrupted $A\beta_{1-40}$ fibril formation by a similar degree. The other AAMPs (AAMP-0 and Dpg-containing AAMP-6) reduced$A\beta_{1-40}$ ThT fluorescence by ∼20%. Interestingly, these were the mitigators that only altered fibril morphology when aged with monomeric $A\beta_{1-40}$. The reduced fluorescence observed could also be from inhibitor molecules displacing ThT molecules bound to the preformed fibrils leading to false positive results for fibril disassembly (*63*, *82*). Thus, AFM and TEM were used to probe the morphology of the $A\beta_{1-40}$ disassembly products.

Size and Morphology of Structures Formed from Disassembly of Preformed Fibrils by Various AAMPs

Results for the disassembly of preformed fibrils by 24 h incubation with certain AAMPs are summarized in Table 3. A topographic AFM image of $A\beta_{1-40}$ taken after 6 days aging showed a dense network of fibrils (Figure 7A) with a mean height of 6 ± 3 nm. The height analysis (Figure 7B) reveals the maturity of the fibrils formed, with more than 60% of the fibrils having heights between 4 and 8 nm, consistent with the height of mature fibrils (7−10 nm).

Topographic AFM images of $A\beta_{1-40}$ fibrils disassembled by AAMP-0 (no ααAAs) exhibit reduced surface coverage of fibrils and a few spherical particles consistent with the 20% reduction in ThT fluorescence observed relative to that of $A\beta_{1-40}$. Also, this is consistent

DOI: 10.1021/cn100045q | *ACS Chem. Neurosci.* (2010), *1*, 608–626

with previous reports that AAMP-0 does not induce fibril disassembly. The height distribution shows a distribution similar to that of Aβ_{1-40} fibrils (Figure 7D). In contrast, ααAA-containing AAMPs induced disassembly of preformed fibrils to form nonfibrillic assemblies and isolated protofibrils/fibrils. Nonfibrillic assemblies and a few isolated fibrillar structures were the main structures observed from Aβ_{1-40} fibril disassembly by AAMP-1 (Figure 7E), with three ααAAs. The same result (nonfibrillic assemblies) was also observed with AAMP-2 (Figure 7G), AAMP-3 (Figure 7I), and AAMP-4 (Figure 7K), incorporating two ααAAs compared with AAMP-1. In addition to observing nonfibrillic assemblies, isolated protofibrils (beaded morphology) and fibrils (smooth) were detected in these mixtures. The height distribution reveals that most of the particles formed were less than 10 nm in height (Figure 7B,D,F, H,J,L). Coincidentally, these same AAMPs showed up to 80% reduction in ThT fluorescence. Thus, ααAAs play a role in disassembly of preformed fibrils as seen from fibrils being the predominant species formed with AAMP-0 (no ααAAs) compared with nonfibrillic assemblies formed with ααAA-containing AAMPs, for example AAMP-1, AAMP-2, etc. This is consistent

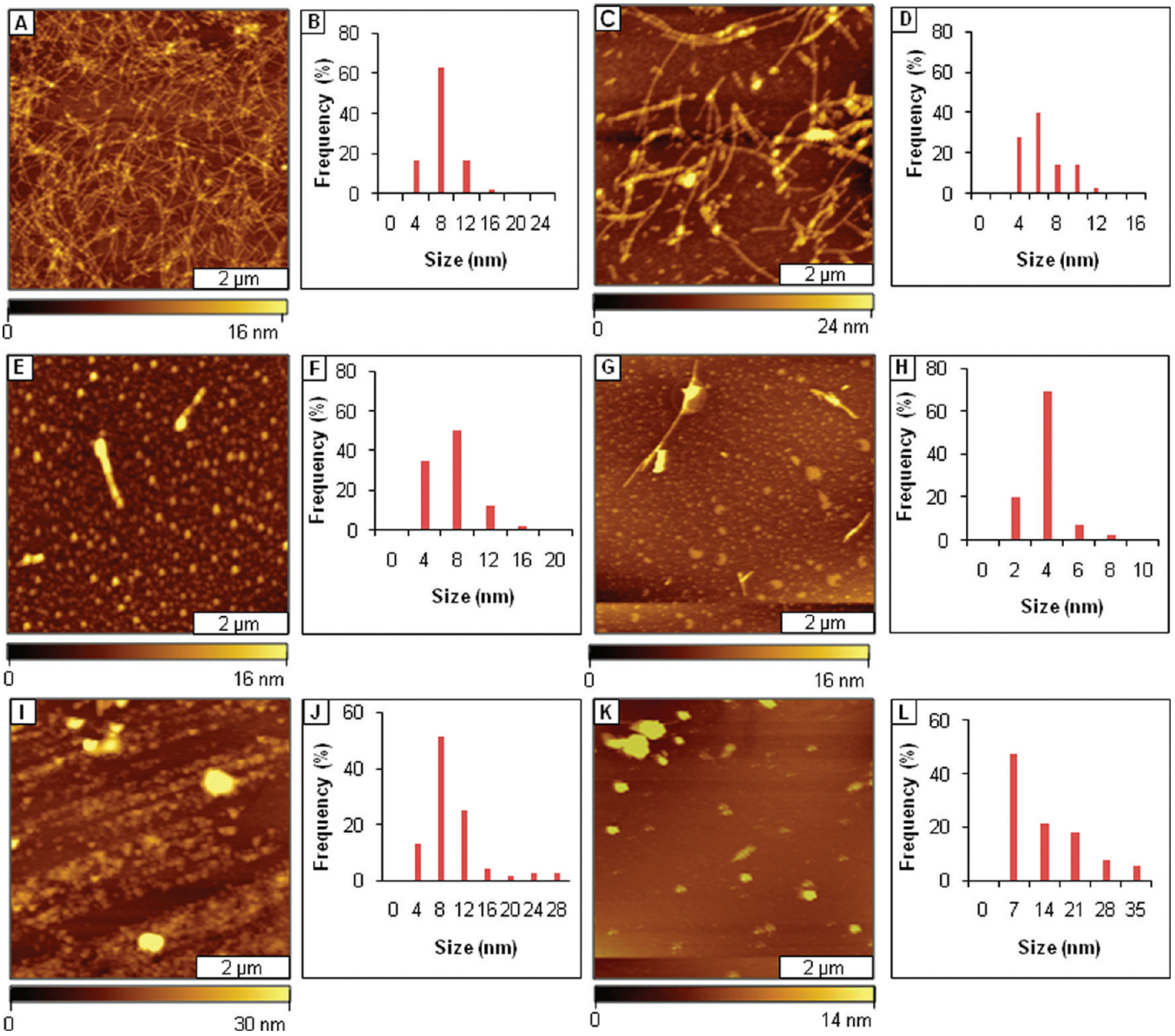

Figure 7. Disassembly of Aβ_{1-40} preformed fibrils: (A) Aβ_{1-40} fibrils; (B) corresponding histogram; (C) fibrils/protofibrils formed as a result of fibril disassembly after 24 h exposure to AAMP-0; (D) height analysis for panel C; (E) spherical aggregates induced by 24 h exposure to AAMP-1 fibril to induce disassembly; (F) height histogram analysis for panel E; (G) spherical particles formed after 24 h disassembly by AAMP-2; (H) height analysis for panel G; (I) spherical aggregates from disassembly by AAMP-3 after 24 h; (J) corresponding height analysis; (K) spherical assemblies formed from fibril disassembly by AAMP-4 after 24 h; (L) height histogram for panel K.

DOI: 10.1021/cn100045q | ACS Chem. Neurosci. (2010), 1, 608–626

with the ThT fluorescence observations. Significant also was the increased heights of isolated fibrils formed by disassembly of preformed fibrils by ααAA-containing AAMPs compared with either Aβ_{1-40} fibrils or AAMP-0 (Table 1). This may suggest that ααAAMPs bind to fibrils or cause the fibrils to coalesce resulting in increased heights.

Disassembly by 24 h incubation of preformed fibrils with AAMPs having one ααAA resulted in mixtures of spherical particles and protofibrils/fibrils. For instance, spherical particles and isolated fibrils/protofibrils were formed from Aβ_{1-40} fibril disassembly by AAMP-5 (Figure 8A), AAMP-7 (Figure 8E), and AAMP-8 (Figure 8G). In contrast, disassembly of preformed fibrils by AAMP-6 formed mainly fibrillar structures (Figure 8C) that exhibited a beaded morphology and a periodicity characteristic of protofibrils.

Larger spherical particles were formed from disassembly by AAMP-7 and AAMP-8 compared with AAMP-5, as shown by the height analysis (Figure 8B, F,H). Surprisingly, similar trends were observed for the assembly of Aβ_{1-40} in the presence of these AAMPs and thus aromaticity (AAMP-7) and steric effects (AAMP-8) play a part in the disassembly process as well. Isolated protofibrils/fibrils, observed along with spherical particles for AAMP-7 and AAMP-8, were shorter in length and in some with beaded morphology compared with Aβ_{1-40} fibrils. Also, the protofibrils/fibrils formed by AAMP-6 were shorter and with beaded morphology but with similar height distribution (Figure 8D) and mean height (Table 2) compared with Aβ_{1-40} fibrils. This suggests that these AAMPs induced partial disassembly or fibril breakage of preformed fibrils forming protofibrils (beaded morphology) and short fibrils with mean heights matching those of Aβ_{1-40} fibrils (Table 2). The partial disassembly of Aβ_{1-40} preformed fibrils and disruption of fibril formation by AAMP-6 shows that positioning of ααAAs relative to KLVFF influences both disassembly and assembly processes.

The observed disassembly of preformed fibrils into either oligomeric or prefibrillar particles (precursors of fibril formation) indicates a shift in equilibrium. It has been shown that fibrils elongate by monomer addition to the fibril ends. Therefore, disassembly of fibrils suggests that AAMP possibly binds at the fibril end, which shifts the thermodynamic equilibrium back toward oligomeric (AAMP-5, AAMP-7, and AAMP-8) and protofibrillar (AAMP-6) assemblies. Even in cases where fibrils/protofibrils were observed, the surface coverage was profoundly reduced compared with the dense network of

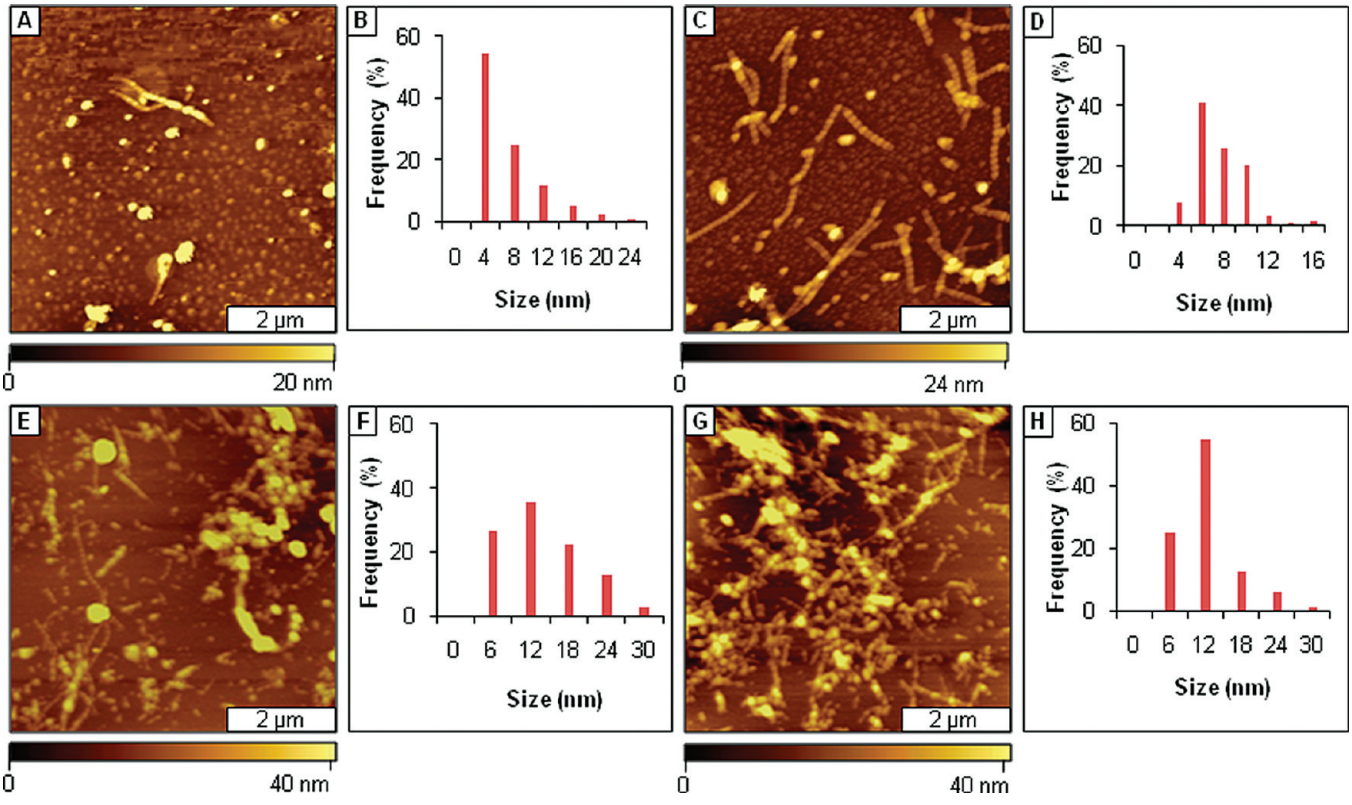

Figure 8. Disassembly of Aβ_{1-40} preformed fibrils after 24 h exposure to certain AAMPs: (A) spherical aggregates induced by AAMP-5 fibril disassembly; (B) height histogram analysis for panel A; (C) fibrils/protofibrils formed as a result of fibril disassembly by AAMP-6; (D) height analysis for panel C; (E) spherical aggregates from disassembly by AAMP-7; (F) corresponding height analysis; (G) spherical assemblies formed from fibril disassembly by AAMP-8; (H) height histogram for panel G.

DOI: 10.1021/cn100045q | ACS Chem. Neurosci. (2010), 1, 608–626

$A\beta_{1-40}$ fibrils, suggesting that some amount of disassembly occurred.

Conclusions

Our study validates the use of ααAAs as disrupting elements when incorporated into the KLVFF motif for designing amyloid aggregation mitigating peptides, as indicated by the absence of fibrillic assemblies in comparison to the control peptide (AAMP-0). We showed that the side-chain interactions associated with the various ααAAs are important in disrupting fibril formation. A major finding was that the mitigators possessing one ααAA were as effective in disrupting $A\beta_{1-40}$ fibril formation as the mitigators having two or three ααAAs. Thus, these findings support our efforts to reduce the overall molecular weight of the peptide without affecting its efficacy for optimal in vivo use and improved systemic bioavailability.

Interestingly, we found that the mitigators that disrupted fibril formation also disassembled fibrils. This suggests the existence of an equilibrium between $A\beta_{1-40}$ monomers/dimers and fibrils. Molecular dynamic simulations have been employed to study the mechanism of how these mitigators interact and disassemble fibrils (*80*, *83*, *84*). Recently, Yassmine et al. showed through simulation the disassembly of $A\beta_{16-22}$ protofibrils by *N*-methylated inhibitors (*85*). They reported that *N*-methylated inhibitors interact with the protofibril by both lateral and longitudinal association, thereby disrupting the β-sheet extension and its lateral association into layers. More importantly, they showed that the inhibitor peptides intercalate and possibly sequester the $A\beta$ peptides, which we believe to be the mode of action for our designed ααAA-AAMPs in disrupting $A\beta_{1-40}$ fibrillogenesis. The substoichiometric inhibition of fibril formation by selected mitigators is further evidence for this mode of action. Based on Tycko's structural model (*86*), we hypothesize that the interaction of ααAA-AAMPs with $A\beta_{1-40}$ at the region 17−20 disrupts the "bend" segment between the two β-strands, affecting β-sheet extension and packing during fibril formation.

More recently, the fibril growth mechanism has been shown in computer simulations and experimental data to proceed via two steps (*87*, *88*). The initial step is coalescence driven by the rapid formation of nonspecific hydrophobic interactions. This is followed by a conformational conversion to ordered β-sheet structures because of the slow formation of highly directional, interchain hydrogen bonds. Competition between hydrophobic interactions and hydrogen bonding is important for determining the morphology of aggregates that are formed. Aging conditions can affect hydrogen-bonding interactions to yield both fibrillar and nonfibrillar assemblies with different morphologies but with the same β-sheet content. Based on our design strategy, we hypothesized that AAMPs bind $A\beta_{1-40}$ and block one face of aggregation, which affects the formation of hydrogen-bonding interchains and takes $A\beta_{1-40}$ fibrillogenesis off the normal aggregation pathway. This favors hydrophobic interactions over hydrogen bonding and results in nonfibrillic assemblies. In addition, the absence of fibrillar structures in aged $A\beta$ mitigator solutions is evidence that supports a mechanism of growth by coalescence and conversion into β-sheet-rich assemblies. This differs in comparison to a nucleation-dependent mechanism, where inhibitor would act as seed and enhance aggregation kinetics leading primarily to formation of fibrils; since such fibrils were not the major species observed in most of the experiments.

Based on recent reports that show oligomers to be more toxic than fibrils, the spherical particles formed from our $A\beta$ assembly mitigation experiments are also expected to be toxic. However, not all oligomers are toxic, probably because of the size distribution over a wide molecular weight range (less than 10 kDa to greater than 100 kDa), and with structural polymorphism observed even with oligomers of similar sizes. This indicates that the size, morphology, and on/off pathway are possible factors that determine the toxicity of oligomers. We hypothesize that the spherical $A\beta$−inhibitor aggregate is an off-pathway product and very likely is different morphologically than normal $A\beta$ oligomer aggregate and hence is less toxic. This hypothesis is supported by reports that show inhibitors that alter $A\beta$ aggregation kinetics form morphologically different fibrils that are less toxic.

Furthermore, a possible application of our findings is that ααAAs can be used to control neuronal toxicity from $A\beta$ species. Neurotoxicity is believed to be a result of aberrant interactions between cellular components, such as membranes, proteasomes, or molecular chaperons, and solvent-exposed hydrophobic surfaces of oligomeric assemblies. The size of aggregates affects these interactions, with the highest toxicity resulting from aggregates with a high surface area to volume ratio (*89*−*91*). This explains why fibrils and, to some extent, large oligomers are not very toxic compared with small oligomeric assemblies. We showed that position, distribution, and side-chain functionality of ααAAs incorporated in the binding core affects the size of the resulting assemblies. Thus, we can use ααAAs to influence the desired size of aggregates formed, in hopes of controlling neurotoxicity. This hypothesis will be tested as part of the future work in cellular systems.

Methods

Reagents

The 40-mer peptide ($A\beta_{1-40}$) was purchased from Invitrogen Corporation, (Carlsbad, CA)

DOI: 10.1021/cn100045q | *ACS Chem. Neurosci.* (2010), *1*, 608–626

Peptide Synthesis

Samples of AAMPs were prepared from 9*H*-fluoren-9-ylmethoxycarbonyl (Fmoc) amino acids using solid-phase peptide synthesis (SPSS) on PAL-PEG-PS resin or Rink amide ChemMatrix resin. Couplings, Fmoc removal, and resin cleavage were carried out using previously described methods (*92*−*94*). The crude peptides were purified by reversed-phase HPLC using a 10% to 70% B linear gradient over 60 min [Waters C_4 100 Å column using solvent A (water and 0.1% trifluoroacetic acid, TFA) and solvent B (acetonitrile and 0.1% TFA)]. The purity of the peptides was evaluated by analytical HPLC, and the identity of the peptides was assigned from masses determined by ESI-MS. The percent peptide content was established by amino acid analysis.

Peptide Monomerization

Lyophilized Aβ_{1-40} was pretreated to form monomeric solutions following our previously published protocol (*71*). Briefly, Aβ_{1-40} was dissolved in neat TFA at 1 mg mL^{-1} and sonicated for 10−20 min. Removal of TFA using a Centrivac yielded a pale yellowish residue, and it was redissolved in 1 mL of hexafluoroisopropanol (HFIP) at 1 mg mL^{-1} and then incubated at 37 °C for 1 h. Removal of HFIP yielded a white powder that was redissolved in HFIP and split into 0.25 mg fractions based on the assumption that the mass of Aβ_{1-40} was 50% at this point in the preparation. The fractions were incubated for 1 h, at which time the HFIP was removed by vacuum, and the resulting white powder was lyophilized overnight. The lyophilized white powder was dissolved in a 2×10^{-3} M NaOH/PBS (100 mM, 300 mM NaCl, pH 7.4) mixture at a 1:1 ratio and then centrifuged for 20 min at 13 000 × *g*; these solutions were used immediately in aggregation assays. The supernatant was subjected to amino acid analysis to determine the net peptide content of the solutions.

Thioflavin T Aggregation Assays

Monomeric Aβ_{1-40} prepared as described in the peptide monomerization section was aged alone and in the presence of AAMPs at 37 °C while shaking (Brinkmann Eppendorf Thermomixer, model 21516-170 operated at 300 rpm) in phosphate-buffered saline (PBS) buffer (50 mM, 150 mM NaCl, pH 7.4). For ThT results from longer time points of 3 months, samples were incubated at 37 °C for 7 days and then were aged further at room temperature under nitrogen. At various time points, 10 μL of sample, 10 μL of 100 μM ThT stock solution in water, and 180 μL of PBS were mixed in a low-binding, 96-well plate with a transparent bottom (Corning incorporated cat. no. 3651). A ThT fluorescence emission spectrum was acquired at 480 nm (excitation at 440 nm) using a fluorescence plate reader (BMG, LABTECH).

Circular Dichroism

Monomeric samples of Aβ_{1-40} were aged alone and with equimolar AAMP at 37 °C for several days while shaking. The CD spectra were recorded at room temperature on an Aviv CD spectrometer.

Atomic Force Microscopy

A sample aliquot of 10 μL was diluted 2-fold and adsorbed onto the surface of freshly cleaved mica(0001) for 5−10 min (Ruby muscovite mica, S&J Trading Co., NY). The remaining excess liquid was absorbed onto a filter paper or lab tissue. Salts and excess unbound peptide were removed by rinsing the surface three times with 40 μL of deionized water. An Agilent 5500 atomic force microscope equipped with PicoScan v5.3.3 software was used for surface characterizations (Agilent Technologies AFM, Inc. Chandler, AZ). Cantilevers (NSL-20) from Nanoworld Holdings AG (Schaffhausen, Switzerland) were used for imaging samples by tapping mode in air. The cantilever was driven to oscillate at 185 ± 10 kHz for ambient AFM characterizations. The mean height is obtained by taking multiple cursor measurements of the thickness of the fibrils throughout several representative images. The distribution of heights is presented as a histogram for each AFM view. The individual plots shown for the surface topography of the various samples are representative views of the morphologies observed for multiple areas of the samples.

Transmission Electron Microscopy

Samples for TEM analysis were prepared by placing sample droplet onto a carbon support Cu-coated grid (EMS 400-CU) for 1−2 min. Excess sample was absorbed into a filter paper, placed onto a droplet of water, and then stained using 2% uranyl acetate droplet. The grid was cleared of excess uranyl acetate, labeled with its experimental designation, and then stored in a Petri dish. Images were recorded using a JEOL 100 CX TEM, 80 kV accelerating voltage.

Supporting Information Available

Additional data including extended figures. This material is available free of charge via the Internet at http://pubs.acs.org.

Author Information

Corresponding Author

* Jayne C. Garno: phone 225-578-8942; e-mail jgarno@lsu.edu; mailing address Chemistry Department, Louisiana State University, 232 Choppin Hall, Baton Rouge, LA 70803.

Author Contributions

Experiment design, peptide synthesis and CD characterizations were accomplished by C.K.B., K.R.F., and R.P.H. Characterizations with AFM were accomplished by J.N.N. and C.K.B. with instruments and materials provided by J.C.G. Data analysis and writing were completed by C.K.B. with editing and analysis by all of the authors.

Funding Sources

Funding for this work was provided by the Louisiana Board of Regents (Grant LEQSF(2006-09)-RD-A-04) and the National Science Foundation Career Program (Grant CHE-0847291).

Acknowledgment

W.K.S. is an LSU doctoral candidate on study-leave from Masinde Muliro University, Kenya.

Abbreviations

AD, Alzheimer's disease; AAMPs, amyloid aggregation mitigating peptides; Aβ, β-amyloid peptide; AFM, atomic force

microscopy; ααAAs, α,α disubstituted amino acids; APP, amyloid precursor protein; CD, circular dichroism; Dbg, dibenzylglycine; Dibg, diisobutyl-glycine; Dpg, dipropyl glycine; Fmoc, 9*H*-fluoren-9-ylmethoxycarbonyl; HAM, hierarchical assembly model; HFIP, hexafluoroisopropanol; HPLC, high-performance liquid chromatography; PBS, phosphate-buffered saline; SPSS, solid-phase peptide synthesis; TEM, transmission electron microscopy; TFA, trifluoroacetic acid; ThT, thioflavin T dye.

References

1. Selkoe, D. J. (1991) The molecular pathology of Alzheimers-Disease. *Neuron 6*, 487–498.

2. Hardy, J., and Selkoe, D. J. (2002) Medicine - The amyloid hypothesis of Alzheimer's disease: Progress and problems on the road to therapeutics. *Science 297*, 353–356.

3. Selkoe, D. J. (2002) Alzheimer's disease is a synaptic failure. *Science 298*, 789–791.

4. Sengupta, P., Garai, K., Sahoo, B., Shi, Y., Callaway, D. J. E., and Maiti, S. (2003) The amyloid β peptide ($A\beta_{1-40}$) is thermodynamically soluble at physiological concentrations. *Biochemistry 42*, 10506–10513.

5. Bieschke, J., Zhang, Q. H., Powers, E. T., Lerner, R. A., and Kelly, J. W. (2005) Oxidative metabolites accelerate Alzheimer's amyloidogenesis by a two-step mechanism, eliminating the requirement for nucleation. *Biochemistry 44*, 4977–4983.

6. Harper, J. D., and Lansbury, P. T. (1997) Models of amyloid seeding in Alzheimier's disease and scrapie: Mechanistic truths and physiological consequences of the time-dependent solubility of amyloid proteins. *Annu. Rev. Biochem. 66*, 385–407.

7. Zhang, Q. H., Powers, E. T., Nieva, J., Huff, M. E., Dendle, M. A., Bieschke, J., Glabe, C. G., Eschenmoser, A., Wentworth, P., Lerner, R. A., and Kelly, J. W. (2004) Metabolite-initiated protein misfolding may trigger Alzheimer's disease. *Proc. Natl. Acad. Sci. U.S.A. 101*, 4752–4757.

8. Lansbury, P. T.Jr. (1997) Inhibition of amyloid formation: A strategy to delay the onset of Alzheimer's disease. *Curr. Opin. Chem. Biol. 1*, 260–267.

9. Walsh, D. M., and Selkoe, D. J. (2007) A beta Oligomers - a decade of discovery. *J. Neurochem. 101*, 1172–1184.

10. Stefani, M., and Dobson, C. M. (2003) Protein aggregation and aggregate toxicity: new insights into protein folding, misfolding diseases and biological evolution. *J. Mol. Med. 81*, 678–699.

11. Hartley, D. M., Walsh, D. M., Ye, C. P., Diehl, T., Vasquez, S., Vassilev, P. M., Teplow, D. B., and Selkoe, D. J. (1999) Protofibrillar intermediates of amyloid beta-protein induce acute electrophysiological changes and progressive neurotoxicity in cortical neurons. *J. Neurosci. 19*, 8876–8884.

12. Walsh, D. M., Townsend, M., Podlisny, M. B., Shankar, G. M., Fadeeva, J. V., El Agnaf, O., Hartley, D. M., and Selkoe, D. J. (2005) Certain inhibitors of synthetic amyloid beta - peptide (Abeta) fibrillogenesis block oligomerization of natural Abeta and thereby rescue long-term potentiation. [Erratum to document cited in CA143:090706], *J. Neurosci. 25*, No pp given.

13. Haass, C., and Selkoe, D. J. (2007) Soluble protein oligomers in neurodegeneration: Lessons from the Alzheimer's amyloid beta-peptide. *Nat. Rev. Mol. Cell Biol. 8*, 101–112.

14. Lee, S., Fernandez, E. J., and Good, T. A. (2007) Role of aggregation conditions in structure, stability, and toxicity of intermediates in the A beta fibril formation pathway. *Protein Sci. 16*, 723–732.

15. Lee, S., Carson, K., Rice-Ficht, A., and Good, T. (2005) Hsp20, a novel alpha-crystallin, prevents A beta fibril formation and toxicity. *Protein Sci. 14*, 593–601.

16. Walsh, D. M., and Selkoe, D. J. (2004) Oligomers in the brain: The emerging role of soluble protein aggregates in neurodegeneration. *Protein Pept. Lett. 11*, 213–228.

17. Reed, M. N., Hofmeister, J. J., Jungbauer, L., Welzel, A. T., Yu, C., Sherman, M. A., Lesné, S., LaDu, M. J., Walsh, D. M., Ashe, K. H., and Cleary, J. P. Cognitive effects of cell-derived and synthetically derived A[beta] oligomers, *Neurobiol. Aging* in press.

18. Selkoe, D. J. (2008) Soluble oligomers of the amyloid [beta]-protein impair synaptic plasticity and behavior. *Behav. Brain Res. 192*, 106–113.

19. Masafumi, S., and Tamotsu, Z. (2010) Amyloid oligomers: Formation and toxicity of Aβ oligomers. *FEBS J. 277*, 1348–1358.

20. Walsh, D. M., and Selkoe, D. J. (2004) Oligomers in the brain: The emerging role of soluble protein aggregates in neurodegeneration. *Protein Pept. Lett. 11*, 213–228.

21. Chauhan, V., and Chauhan, A. (2006) Oxidative stress in Alzheimer's disease. *Pathophysiology 13*, 195–208.

22. Su, Y., and Chang, P.-T. (2001) Acidic pH promotes the formation of toxic fibrils from [beta]-amyloid peptide. *Brain Res. 893*, 287–291.

23. Findeis, M. A. (2000) Approaches to discovery and characterization of inhibitors of amyloid [beta]-peptide polymerization. *Biochim. Biophys. Acta, Mol. Basis Dis. 1502*, 76–84.

24. Findeis, M. A. (2007) The role of amyloid [beta] peptide 42 in Alzheimer's disease. *Pharmacol. Ther. 116*, 266–286.

25. Kornilova, A. Y., and Wolfe, M. S. (2003) Secretase inhibitors for Alzheimer's disease. *Annu. Rep. Med. Chem.* 41–50.

26. Shelton, C. C., Zhu, L., Chau, D., Yang, L., Wang, R., Djaballah, H., Zheng, H., and Li, Y.-M. (2009) Modulation of gamma-secretase specificity using small molecule allosteric inhibitors. *Proc. Natl. Acad. Sci. U.S.A. 106*, 20228–20233.

27. Kreft, A. F., Martone, R., and Porte, A. (2009) Recent advances in the identification of gamma-secretase inhibitors to clinically test the A-β oligomer hypothesis of Alzheimer's disease. *J. Med. Chem. 52*, 6169–6188.

28. Bard, F., Cannon, C., Barbour, R., Burke, R. L., Games, D., Grajeda, H., Guido, T., Hu, K., Huang, J. P., Johnson-Wood, K., Khan, K., Kholodenko, D., Lee, M., Lieberburg, I., Motter, R., Nguyen, M., Soriano, F., Vasquez, N., Weiss, K., Welch, B., Seubert, P., Schenk, D., and Yednock, T. (2000) Peripherally administered antibodies against amyloid beta-peptide enter the central nervous system and reduce pathology in a mouse model of Alzheimer disease. *Nat. Med. 6*, 916–919.

DOI: 10.1021/cn100045q | *ACS Chem. Neurosci.* (2010), *1*, 608–626

29. Bard, F., Barbour, R., Cannon, C., Carretto, R., Fox, M., Games, D., Guido, T., Hoenow, K., Hu, K., Johnson-Wood, K., Khan, K., Kholodenko, D., Lee, C., Lee, M., Motter, R., Nguyen, M., Reed, A., Schenk, D., Tang, P., Vasquez, N., Seubert, P., and Yednock, T. (2003) Epitope and isotype specificities of antibodies to beta-amyloid peptide for protection against Alzheimer's disease-like neuropathology. *Proc. Natl. Acad. Sci. U.S.A. 100*, 2023–2028.

30. Dodart, J. C., Bales, K. R., Gannon, K. S., Greene, S. J., DeMattos, R. B., Mathis, C., DeLong, C. A., Wu, S., Wu, X., Holtzman, D. M., and Paul, S. M. (2002) Immunization reverses memory deficits without reducing brain A beta burden in Alzheimer's disease model. *Nat. Neurosci. 5*, 452–457.

31. Komatsu, M., Waguri, S., Chiba, T., Murata, S., Iwata, J., Tanida, I., Ueno, T., Koike, M., Uchiyama, Y., Kominami, E., and Tanaka, K. (2006) Loss of autophagy in the central nervous system causes neurodegeneration in mice. *Nature 441*, 880–884.

32. Cohen, E., Bieschke, J., Perciavalle, R. M., Kelly, J. W., and Dillin, A. (2006) Opposing activities protect against age-onset proteotoxicity. *Science 313*, 1604–1610.

33. Hara, T., Nakamura, K., Matsui, M., Yamamoto, A., Nakahara, Y., Suzuki-Migishima, R., Yokoyama, M., Mishima, K., Saito, I., Okano, H., and Mizushima, N. (2006) Suppression of basal autophagy in neural cells causes neurodegenerative disease in mice. *Nature 441*, 885–889.

34. Findeis, M. A. (2000) Approaches to discovery and characterization of inhibitors of amyloid beta -peptide polymerization. *Biochim. Biophys. Acta, Mol. Basis Dis. 1502*, 76–84.

35. Sun, Y., Zhang, G., Hawkes, C. A., Shaw, J. E., McLaurin, J., and Nitz, M. (2008) Synthesis of scyllo-inositol derivatives and their effects on amyloid beta peptide aggregation. *Bioorg. Med. Chem. 16*, 7177–7184.

36. Shoval, H., Lichtenberg, D., and Gazit, E. (2007) The molecular mechanisms of the anti-amyloid effects of phenols. *Amyloid 14*, 73–87.

37. Cohen, T., Frydman-Marom, A., Rechter, M., and Gazit, E. (2006) Inhibition of amyloid fibril formation and cytotoxicity by hydroxyindole derivatives. *Biochemistry 45*, 4727–4735.

38. Nitz, M., Fenili, D., Darabie, A., A., Wu, L., Cousins, J., E., and McLaurin, J. (2008) Modulation of amyloid-beta aggregation and toxicity by inosose stereoisomers. *FEBS J. 275*, 1663–1674.

39. Liu, R. T., McAllister, C., Lyubchenko, Y., and Sierks, M. R. (2004) Residues 17−20 and 30−35 of beta-amyloid play critical roles in aggregation. *J. Neurosci. Res. 75*, 162–171.

40. Ghanta, J., Shen, C.-L., Kiessling, L. L., and Murphy, R. M. (1996) A strategy for designing inhibitors of β-amyloid toxicity. *J. Biol. Chem. 271*, 29525–29528.

41. Lowe, T. L., Strzelec, A., Kiessling, L. L., and Murphy, R. M. (2001) Structure−function relationships for inhibitors of β-amyloid toxicity containing the recognition sequence KLVFF. *Biochemistry 40*, 7882–7889.

42. Pallitto, M. M., Ghanta, J., Heinzelman, P., Kiessling, L. L., and Murphy, R. M. (1999) Recognition sequence design for peptidyl modulators of β-amyloid aggregation and toxicity. *Biochemistry 38*, 3570–3578.

43. Lowe, T. L., Strzelec, A., Kiessling, L. L., and Murphy, R. M. (2001) Structure-function relationships for inhibitors of beta-amyloid toxicity containing the recognition sequence KLVFF. *Biochemistry 40*, 7882–7889.

44. Tjernberg, L. O., Naslund, J., Lindqvist, F., Johansson, J., Karlstrom, A. R., Thyberg, J., Terenius, L., and Nordstedt, C. (1996) Arrest of beta-amyloid fibril formation by a pentapeptide ligand. *J. Biol. Chem. 271*, 8545–8548.

45. Sidhartha, M. C., Hinke, M., Maarten, M., Meijer, E. W., David, V., Hilal, A. L., Frank, B., and Wiep, S. (2007) Branched KLVFF Tetramers strongly potentiate inhibition of beta-amyloid aggregation. *ChemBioChem 8*, 1857–1864.

46. Chalifour, R. J., McLaughlin, R. W., Lavoie, L., Morissette, C. l., Tremblay, N., Boulé, M., Sarazin, P., Stéa, D., Lacombe, D., Tremblay, P., and Gervais, F. (2003) Stereoselective interactions of peptide inhibitors with the β-amyloid peptide. *J. Biol. Chem. 278*, 34874–34881.

47. Watanabe, K.-i., Nakamura, K., Akikusa, S., Okada, T., Kodaka, M., Konakahara, T., and Okuno, H. (2002) Inhibitors of fibril formation and cytotoxicity of [beta]-amyloid peptide composed of KLVFF recognition element and flexible hydrophilic disrupting element. *Biochem. Biophys. Res. Commun. 290*, 121–124.

48. Austen, B. M., Paleologou, K. E., Ali, S. A. E., Qureshi, M. M., Allsop, D., and El-Agnaf, O. M. A. (2008) Designing peptide inhibitors for oligomerization and toxicity of Alzheimer's β-amyloid peptide. *Biochemistry 47*, 1984–1992.

49. Gordon, D. J., Sciarretta, K. L., and Meredith, S. C. (2001) Inhibition of β-amyloid(40) fibrillogenesis and disassembly of β-amyloid(40) fibrils by short β-amyloid congeners containing *N*-methyl amino acids at alternate residues. *Biochemistry 40*, 8237–8245.

50. Gordon, D. J., Tappe, R., and Meredith, S. C. (2002) Design and characterization of a membrane permeable N-methyl amino acid-containing peptide that inhibits A. beta.1−40 fibrillogenesis. *J. Pept. Res. 60*, 37–55.

51. Gordon, D. J., and Meredith, S. C. (2003) Probing the role of backbone hydrogen bonding in β-amyloid fibrils with inhibitor peptides containing ester bonds at alternate positions. *Biochemistry 42*, 475–485.

52. Bieschke, J., Siegel, S. J., Fu, Y. W., and Kelly, J. W. (2008) Alzheimer's Aβ peptides containing an isostructural backbone mutation afford distinct aggregate morphologies but analogous cytotoxicity. Evidence for a common low-abundance toxic structure(s). *Biochemistry 47*, 50–59.

53. Fu, Y. W., Gao, J. M., Bieschke, J., Dendle, M. A., and Kelly, J. W. (2006) Amide-to-E-olefin versus amide-to-ester backbone H-bond perturbations: Evaluating the O−O repulsion for extracting H-bond energies. *J. Am. Chem. Soc. 128*, 15948–15949.

54. Soto, C., Sigurdsson, E. M., Morelli, L., Kumar, R. A., Castano, E. M., and Frangione, B. (1998) Beta-sheet breaker peptides inhibit fibrillogenesis in a rat brain model of amyloidosis: Implications for Alzheimer's therapy. *Nat. Med. 4*, 822–826.

DOI: 10.1021/cn100045q | *ACS Chem. Neurosci.* (2010), *1*, 608–626

55. Karle, I. L., and Balaram, P. (1990) Structural characteristics of α-helical peptide molecules containing Aib residues. *Biochemistry 29*, 6747–6756.

56. Etienne, M. A., Aucoin, J. P., Fu, Y. W., McCarley, R. L., and Hammer, R. P. (2006) Stoichiometric inhibition of amyloid beta-protein aggregation with peptides containing alternating α,α-disubstituted amino acids. *J. Am. Chem. Soc. 128*, 3522–3523.

57. Li, Q. Y., Gordon, M., Etienne, M. A., Hammer, R. P., and Morgan, D. (2008) Contrasting in vivo effects of two peptide-based amyloid-beta protein aggregation inhibitors in a transgenic mouse model of amyloid deposition. *Cell Transplant. 17*, 397–408.

58. Pavone, V., Lombardi, A., Saviano, M., De Simone, G., Nastri, F., Maglio, O., Omote, Y., Yamanaka, Y., and Yamada, T. (2000) Conformational behavior of C-alpha,C-alpha-diphenyl glycine: Extended conformation in tripeptides containing consecutive D phi G residues. *Biopolymers 53*, 161–168.

59. Toniolo, C., Crisma, M., Formaggio, F., and Peggion, C. (2001) Control of peptide conformation by the Thorpe-Ingold effect (C-alpha-tetrasubstitution). *Biopolymers 60*, 396–419.

60. Levine, H. (1993) Thioflavine-T interaction with synthetic Alzheimers-disease beta-amyloid peptides - detection of amyloid aggregation in solution. *Protein Sci. 2*, 404–410.

61. LeVine, H.III. (1995) Thioflavine T interaction with amyloid beta -sheet structures. *Amyloid 2*, 1–6.

62. Nilsson, M. R. (2004) Techniques to study amyloid fibril formation in vitro. *Methods 34*, 151–160.

63. Wood, S. J., Maleeff, B., Hart, T., and Wetzel, R. (1996) Physical, morphological and functional differences between pH 5.8 and 7.4 aggregates of the Alzheimer's amyloid peptide A [beta]. *J. Mol. Biol. 256*, 870–877.

64. Legleiter, J., Czilli, D. L., Gitter, B., DeMattos, R. B., Holtzman, D. M., and Kowalewski, T. (2004) Effect of different anti-A beta antibodies on A beta fibrillogenesis as assessed by atomic force microscopy. *J. Mol. Biol. 335*, 997–1006.

65. Kad, N. M., Myers, S. L., Smith, D. P., Smith, D. A., Radford, S. E., and Thomson, N. H. (2003) Hierarchical assembly of beta(2)-microglobulin amyloid in vitro revealed by atomic force microscopy. *J. Mol. Biol. 330*, 785–797.

66. Goldsbury, C., Kistler, J., Aebi, U., Arvinte, T., and Cooper, G. J. S. (1999) Watching amyloid fibrils grow by time-lapse atomic force microscopy. *J. Mol. Biol. 285*, 33–39.

67. Liu, R. T., Yuan, B., Emadi, S., Zameer, A., Schulz, P., McAllister, C., Lyubchenko, Y., Goud, G., and Sierks, M. R. (2004) Single chain variable fragments against beta-amyloid (A beta) can inhibit A beta aggregation and prevent A beta-induced neurotoxicity. *Biochemistry 43*, 6959–6967.

68. Harper, J. D., Wong, S. S., Lieber, C. M., and Lansbury, P. T. (1999) Assembly of Aβ amyloid protofibrils: An in vitro model for a possible early event in Alzheimer's disease. *Biochemistry 38*, 8972–8980.

69. Harper, J. D., Wong, S. S., Lieber, C. M., and Lansbury, P. T. (1997) Observation of metastable A beta amyloid protofibrils by atomic force microscopy. *Chem. Biol. 4*, 119–125.

70. Lomakin, A., Chung, D. S., Benedek, G. B., Kirschner, D. A., and Teplow, D. B. (1996) On the nucleation and growth of amyloid beta-protein fibrils: Detection of nuclei and quantitation of rate constants. *Proc. Natl. Acad. Sci. U. S.A. 93*, 1125–1129.

71. Etienne, M. A., Edwin, N. J., Aucoin, J. P., Russo, P. S., McCarley, R. L., and Hammer, R. P. (2007) beta -Amyloid protein aggregation. *Methods Mol. Biol. (Totowa, NJ, U. S.) 386*, 203–225.

72. Laczko, I., Vass, E., Soos, K., Fulop, L., Zarandi, M., and Penke, B. (2008) Aggregation of A beta(1−42) in the presence of short peptides: Conformational studies. *J. Pept. Sci. 14*, 731–741.

73. Li, Q., Gordon, M., Etienne Marcus, A., Hammer Robert, P., and Morgan, D. (2008) Contrasting in vivo effects of two peptide-based amyloid-beta protein aggregation inhibitors in a transgenic mouse model of amyloid deposition. *Cell Transplant. 17*, 397–408.

74. Ionescu-Zanetti, C., Khurana, R., Gillespie, J. R., Petrick, J. S., Trabachino, L. C., Minert, L. J., Carter, S. A., and Fink, A. L. (1999) Monitoring the assembly of Ig light-chain amyloid fibrils by atomic force microscopy. *Proc. Natl. Acad. Sci. U.S.A. 96*, 13175–13179.

75. Ward, R. V., Jennings, K. H., Jepras, R., Neville, W., Owen, D. E., Hawkins, J., Christie, G., Davis, J. B., George, A., Karran, E. H., and Howlett, D. R. (2000) Fractionation and characterization of oligomeric, protofibrillar and fibrillar forms of beta-amyloid peptide. *Biochem. J. 348*, 137–144.

76. Khurana, R., Ionescu-Zanetti, C., Pope, M., Li, J., Nielson, L., Ramirez-Alvarado, M., Regan, L., Fink, A. L., and Carter, S. A. (2003) A general model for amyloid fibril assembly based on morphological studies using atomic force microscopy. *Biophys. J. 85*, 1135–1144.

77. Gazit, E. (2005) Mechanisms of amyloid fibril self-assembly and inhibition. *FEBS J. 272*, 5971–5978.

78. Gazit, E. (2002) A possible role for pi-stacking in the self-assembly of amyloid fibrils. *FASEB J. 16*, 77–83.

79. Carulla, N., Caddy, G. L., Hall, D. R., Zurdo, J., Gairi, M., Feliz, M., Giralt, E., Robinson, C. V., and Dobson, C. M. (2005) Molecular recycling within amyloid fibrils. *Nature 436*, 554–558.

80. Soto, P., Griffin Mary, A., and Shea, J.-E. (2007) New insights into the mechanism of Alzheimer amyloid-beta fibrillogenesis inhibition by N-methylated peptides. *Biophys. J. 93*, 3015–3025.

81. Sato, T., Kienlen-Campard, P., Ahmed, M., Liu, W., Li, H. L., Elliott, J. I., Aimoto, S., Constantinescu, S. N., Octave, J. N., and Smith, S. O. (2006) Inhibitors of amyloid toxicity based on beta-sheet packing of A beta 40 and A beta 42. *Biochemistry 45*, 5503–5516.

82. Nichols, M. R., Moss, M. A., Reed, D. K., Cratic-McDaniei, S., Hoh, J. H., and Rosenberry, T. L. (2005) Amyloid-beta protofibrils differ from Amyloid-beta aggregates induced in dilute hexafluoroisopropanol in stability and morphology. *J. Biol. Chem. 280*, 2471–2480.

83. Tjernberg, L. O., Lilliehook, C., Callaway, D. J. E., Naslund, J., Hahne, S., Thyberg, J., Terenius, L., and Nordstedt, C. (1997) Controlling amyloid beta-peptide fibril

DOI: 10.1021/cn100045q | *ACS Chem. Neurosci.* (2010), *1*, 608–626

formation with protease-stable ligands. *J. Biol. Chem. 272*, 12601–12605.

84. Chen, Z. J., Krause, G., and Reif, B. (2005) Structure and orientation of peptide inhibitors bound to beta-amyloid fibrils. *J. Mol. Biol. 354*, 760–776.

85. Chebaro, Y., and Derreumaux, P. (2009) Targeting the early steps of Abeta 16−22 protofibril disassembly by N-methylated inhibitors: A numerical study. *Proteins: Struct., Funct., Bioinf. 75*, 442–452.

86. Tycko, R. (2003) Insights into the amyloid folding problem from solid-state NMR. *Biochemistry 42*, 3151–3159.

87. Giovanni, B., and Joan-Emma, S. (2009) Diversity of kinetic pathways in amyloid fibril formation. *J. Chem. Phys. 131*, No. 111102.

88. Cheon, M., Chang, I., Mohanty, S., Luheshi, L. M., Dobson, C. M., Vendruscolo, M., and Favrin, G. (2007) Structural reorganisation and potential toxicity of oligomeric species formed during the assembly of amyloid fibrils. *PLoS Comput. Biol. 3*, No. e173.

89. Mu, Y., and Gao, Y. Q. (2007) Effects of hydrophobic and dipole-dipole interactions on the conformational transitions of a model polypeptide. *J. Chem. Phys. 127*, No. 105102.

90. Kim, W., and Hecht, M. H. (2006) Generic hydrophobic residues are sufficient to promote aggregation of the Alzheimer's A beta 42 peptide. *Proc. Natl. Acad. Sci. U.S.A. 103*, 15824–15829.

91. Raman, B., Chatani, E., Kihara, M., Ban, T., Sakai, M., Hasegawa, K., Naiki, H., Rao, C. M., and Goto, Y. (2005) Critical balance of electrostatic and hydrophobic interactions is required for β_2-microglobulin amyloid fibril growth and stability. *Biochemistry 44*, 1288–1299.

92. Fu, Y. W., and Hammer, R. P. (2002) Efficient acylation of the *N*-terminus of highly hindered *C*-$^{\alpha,\alpha}$-disubstituted amino acids via amino acid symmetrical anhydrides. *Org. Lett. 4*, 237–240.

93. Fu, Y. W., Hammarstrom, L. G. J., Miller, T. J., Fronczek, F. R., McLaughlin, M. L., and Hammer, R. P. (2001) Sterically hindered $C^{\alpha,\alpha}$-disubstituted α-amino acids: Synthesis from α-nitroacetate and incorporation into peptides. *J. Org. Chem. 66*, 7118–7124.

94. Fu, Y. W., Etienne, M. A., and Hammer, R. P. (2003) Facile synthesis of α,α-diisobutylglycine and anchoring its derivatives onto PAL-PEG-PS resin. *J. Org. Chem. 68*, 9854–9857.

DOI: 10.1021/cn100045q | *ACS Chem. Neurosci.* (2010), *1*, 608–626